# Ether phospholipids modulate somatosensory responses by tuning multiple receptor functions in *Drosophila*

**Takuto Suito[1,2*], Kohjiro Nagao[3], Xiangmei Deng[1,2,4], Christian Ganser[2], Takayuki Uchihashi[2,5], Motosuke Tsutsumi[2,6], Tomomi Nemoto[2,4,6], Yuji Hara[7], Makoto Tominaga[1,2,4], Takaaki Sokabe[1,2,4*]**

[1] *Division of Cell Signaling, National Institute for Physiological Sciences, National Institutes of Natural Sciences, Okazaki, Japan.*

[2] *Exploratory Research Center on Life and Living Systems, National Institutes of Natural Sciences, Okazaki, Japan.*

[3] *Department of Biophysical Chemistry, Kyoto Pharmaceutical University, Kyoto, Japan.*

[4] *Graduate Institute for Advanced Studies, SOKENDAI, Hayama, Japan*

[5] *Department of Physics, Nagoya University, Nagoya, Japan*

[6] *Division of Biophotonics, National Institute for Physiological Sciences, National Institutes of Natural Sciences, Okazaki, Japan.*

[7] *School of Pharmaceutical Sciences, University of Shizuoka, Shizuoka, Japan*

*To whom correspondence should be addressed: 5-1 Higashiyama, Okazaki, Aichi 444-8787, Japan, Tel.: 81-564-59-5287; E-mail: suito@nips.ac.jp, sokabe@nips.ac.jp

**ABSTRACT**

Transient receptor potential (TRP) and PIEZO channels are known receptors for physical stimuli such as temperature and mechanical touch in sensory nerves. Since these receptors are localized in the plasma membrane, the regulation of sensory receptor activity by plasma membrane lipids has recently attracted attention. In this study, we focused on ether phospholipids (ePLs), which are abundant in neurons, and analyzed their role in somatosensation using *Drosophila* as a model. Reduced warmth avoidance was observed with ePL synthesizing gene knockout or knockdown in warmth-sensitive TRPA1-expressing neurons. The temperature threshold for *Drosophila* TRPA1 channels significantly decreased in presence of ePLs. In addition, we found that ePLs modulate the mechanosensory behavior and activation properties of the mechanosensitive channel PIEZO. Finally, we revealed that ePLs affect physicochemical properties of the plasma membrane, such as membrane tension and lipid order, in culture cells. Our study identified ePLs as crucial regulators of multiple somatosensation modalities in *Drosophila*. Effects due to alteration of cellular membrane properties and activity modulation of sensory receptors.

## INTRODUCTION

The sensory system is indispensable to detect environmental parameters. Sensory perception is initiated by the activation of sensory receptors in sensory nerves and other type of cells, which convert external stimuli into electrical or chemical signals. Transient receptor potential (TRP) channels[1, 2, 3] and PIEZO channels[4] are considered receptors for physical stimuli such as temperature and mechanical touch, and their roles in sensory processing and the underlying mechanisms[5, 6] have been extensively studied[7].

As these receptors are membrane proteins, the functional interaction between ion channels and membrane lipids has been key for resolving their activation mechanisms and cellular functions[8]. The activity of many TRP channels is regulated by a wide variety of lipid molecules, such as phosphatidylinositol phosphates, fatty acids (FA) and their metabolites, endocannabinoids, lysophospholipids, and sphingolipids[9, 10, 11, 12]. The modes of action of these lipids are either direct or indirect, modulating TRP channel activity positively or negatively depending on cellular context and signaling pathways. Similarly, PIEZO channel activities are modulated by lipids. The activity of PIEZO1 is affected by the enrichment of either saturated or polyunsaturated FA (PUFAs) in membrane phospholipids[13, 14]. Phosphatidylserine (PS) may interact with PIEZO1, and the asymmetric distribution of PS in the lipid bilayer is critical for the channel activity[15]. These tight functional linkages between sensory ion channels and lipid molecules exemplify their importance in cellular functions.

A limited number of studies evaluated the physiological significance of lipid molecules on sensory responses in animals. For example, PUFA-containing phospholipids are highly enriched and play a significant role in the brain[16, 17]. In *C. elegans*, arachidonic acid-containing phospholipids modulate the function of touch receptor neurons[18]. In *Drosophila*, an increase in the content of linoleic acid in sensory neurons changes TRPA1 activity and the preferred temperature of larvae[19]. Recently, it has been reported that linoleic acid increases PIEZO2 activity, and that linoleic acid supplementation improves Angelman Syndrome-associated mechanosensory deficits in mice[14]. These results suggest that lipid molecules may modulate the responsiveness and sensitivity of ion channels, thereby influencing neural function and the consequent physiological outputs.

An interesting lipid species in neural tissues is an ether phospholipid (ePL) identified in cancer cells in the 1960s[20]. ePLs constitute 20% of the lipid content in the mouse central nervous

system (CNS) appearing as plasmalogen-type phosphatidylethanolamine (PE), which harbors a vinyl–ether bond at the *sn*-1 position of the glycerol backbone[21]. ePLs are synthesized from dihydroxyacetone phosphate in the peroxisome and transported to the endoplasmic reticulum for further processing. Deficiency in synthesis enzymes of ePLs such as alkylglycerone phosphate synthase (AGPS) can cause rhizomelic chondrodysplasia punctata[22], a peroxisomal disorder resulting in diverse developmental dysfunctions, including neuronal disorders[23]. In addition, ePLs have been implicated in neurodegenerative diseases; lower plasmalogen ePL content has been reported in Alzheimer's disease, Parkinson's disease, Huntington's disease, etc[23]. Although the causal relationship between disease progression and the reduction of ePLs has not been clarified, ePLs may be a functionally important component in the CNS. In the peripheral nervous system, conversely, there is so far no evidence as to the existence and function of ePLs.

Here, we combined lipidomic, behavioral, electrophysiological analyses, and measurements of the physicochemical properties of cell membranes to demonstrate the functional linkage between ePLs and sensory functions in *Drosophila*. Lipid analysis revealed the existence of ePLs, particularly ether phosphatidylethanolamines (ePEs), in neural tissues. Then, we analyzed thermoregulatory behaviors in larvae and found that an *AGPS* knockout or knockdown in warm-sensitive, TRPA1-expressing neurons decreased warmth avoidance. Electrophysiological analyses of TRPA1 revealed the effect of ePLs on lowering the temperature threshold for TRPA1 activation. In addition, we found that *AGPS* knockout or knockdown in mechanosensitive, PIEZO-expressing neurons decreased mechanical nociception. This was caused by a decreased mechano–sensitivity of PIEZO in the absence of ePLs, since we observed enhanced PIEZO activation by ePLs *in vitro*. Finally, we analyzed the effects of ePLs on the physicochemical properties of cell membranes and found that ePLs altered membrane tension and lipid order. Our work demonstrates that ePLs play pivotal roles in optimizing multiple somatosensory modalities by altering cell membrane properties and tuning functions of distinct receptors.

## RESULTS

### *Ether phospholipids are enriched in Drosophila neurons*

Given the limited number of studies reporting ePLs synthesis in *Drosophila melanogaster*, we first confirmed the presence of ePLs in different tissues. We dissected various tissues from third instar larvae or used the whole body to quantify mRNA expression level of *AGPS*, an essential enzyme for ePL biosynthesis[24] (Fig. 1a). *AGPS* was abundantly expressed in the CNS (4.5 times more than in whole body), whereas trace levels of expression were observed in the fat body and carcass (Fig. 1a). *AGPS* expression was also analyzed in peripheral sensory neurons in the body wall. Using magnetic-bead-based cell sorting, we isolated *ppk*-positive sensory neurons, a subset of polymodal, class IV multidendrtic neurons[25]. The *AGPS* expression level in the magnetic bead-bound (class IV neuron enriched) fraction was significantly higher than in the bead unbound (other cells from the body wall) fraction ($p < 0.01$ in Student's t-test, Fig. 1b). These findings suggest that ePL plays functional roles in central and peripheral neurons in *Drosophila*.

Next, to determine ePL composition in *Drosophila* membrane phospholipids, we performed a comprehensive lipid analysis of phospholipid species, including ePLs, in the whole body and the CNS. Specifically, two major classes of phospholipids in *Drosophila*[26], PE and phosphatidylcholine (PC), were analyzed (Fig. 1c–e, Supplementary Fig. 1a, b, Supplementary Table 1–4). The proportion of ePEs in total PEs was 0.64% ± 0.08% in the whole body and 16.6% ± 1.5% in the CNS (Fig. 1c, d). In contrast, only trace level of ether PCs (ePCs) were observed in the PC for both the whole body and the CNS (Fig. 1e and Supplementary Table 2, 4).

Next, we established *AGPS* knockouts (*AGPS* KO) using CRISPR-Cas9 to confirm the functional roles of AGPS in ePL synthesis (Supplementary Fig. 1c). Homozygous *AGPS* KO flies ($AGPS^{KO}$) expressed a negligible level of *AGPS* mRNA (Supplementary Fig. 1d), without obvious growth defects such as a delay in pupariation timing (Supplementary Fig. 1e). The lipid analysis clearly demonstrated complete depletion of ePL molecules in both the whole body and the CNS of $AGPS^{KO}$ (Fig. 1c–e, Supplementary Fig. 1a, b, Supplementary Table 1–4), emphasizing the essential role of *AGPS* in ePL synthesis in *Drosophila*. *AGPS* heterozygous KO flies ($AGPS^{KO/+}$) showed a significant reduction in *AGPS* expression level ($p < 0.001$ in Student's t-test, Supplementary Fig. 1d) but no changes in the total amount of ePLs compared to control (Fig. 1c, Supplementary Fig. 1a, b, Supplementary Table 1, 2).

125 In mammals, the major ePL molecule is of the plasmalogen type, in which an *sn*-1 acyl
126 chain is attached to the glycerol backbone via a vinyl–ether bond. To identify the *sn*-1 and *sn*-2
127 acyl chain profiles of ePEs in *Drosophila*, we performed product ion scan analysis for major ePEs
128 including ePE (34:1), ePE (36:1), ePE (36:2), and ePE (36:3) in the CNS sample (Supplementary
129 Fig. 2a–j). ePE (36:2) appeared to be the most abundant among all ePEs in *Drosophila*'s CNS (Fig.
130 1d). The major product ion of ePE (36:2) coincided with linoleic acid (C18:2) (Supplementary Fig.
131 2h), indicating that the *sn*-2 ester-bound acyl group is C18:2, and the ether-linked *sn*-1 hydrocarbon
132 chain was octadecyl alcohol without double bonds (O-18:0). The other analyzed ePEs harbored
133 either palmitoleic acid (C16:1), oleic acid (C18:1), or linolenic acid (C18:3) at the ester-linked
134 acyl chain, and O-18:0 at the ether-linked acyl chain (Supplementary Fig. 2b, e, j). These data
135 suggested that ePLs, especially ePEs, are abundantly present in *Drosophila* neurons. Moreover,
136 ePEs in *Drosophila* neurons appear to contain an ether bond, but not a vinyl–ether bond, at the *sn-*
137 *1* position, in contrast to the most common ePL molecule found in mammals.
138
139 ***AGPS mutation alters thermoregulatory behaviors in Drosophila***
140 A previous study reported that alterations in membrane lipid composition can affect temperature
141 preference in *Drosophila*[19]. Since ePLs may modulate the physicochemical properties of the
142 plasma membrane, we hypothesized that ePL synthesis should affect sensory responses,
143 particularly to physical stimuli. Therefore, we first investigated the effect of ePLs on
144 thermosensation in larvae. We subjected late third instar larvae (120 hr after egg laying, AEL) to a
145 temperature gradient assay (8ºC–35ºC) to examine their thermotactic behavior. Control ($w^{1118}$) and
146 heterozygous $AGPS^{KO/+}$ larvae distributed through the temperature gradient with peaks around
147 20ºC, avoiding lower and higher temperatures (Fig. 2a). However, two independent clones of
148 *AGPS* homozygous KO ($AGPS^{KO1/KO1}$ and $AGPS^{KO2/KO2}$) lost a clear peak in their distribution,
149 showing increased fractions in high temperature zones than the control and $AGPS^{KO/+}$ larvae (Fig.
150 2a). Specifically, the proportion of larvae distributed over 25ºC zones was 15.5% ± 1.8% in control,
151 whereas significant increases (>30%) were observed in $AGPS^{KO}$ clones (35.8% ± 3.8% in
152 $AGPS^{KO1/KO1}$, 33.0% ± 4.0% in $AGPS^{KO2/KO2}$; $p < 0.001$ in Mann–Whitney U-test, Fig. 2b). These
153 results demonstrated that ePL loss leads to an abnormal thermotactic phenotype in *Drosophila*.
154 To investigate whether sensory functions are affected by the absence of ePLs, we used
155 the GAL4-UAS system for tissue specific *AGPS* knockdown in thermosensory neurons reported

156 to express TRP channels involved in thermotactic behaviors. We used GAL4 lines labeling TRPA1-
157 positive neurons involved in warm temperature avoidance[27] and lines labeling TRPL-[28] and
158 Inactive (Iav)-positive neurons[29] involved in cool temperature avoidance. Among them, *TRPA1-*
159 *AB*$^{GAL4}$-induced *AGPS* knockdown resulted in a significant increase in the fraction of larvae
160 distributed in high temperature zones ($p < 0.001$ in Mann–Whitney U-test, Fig. 2c, d), which
161 resembled the *AGPS*$^{KO}$ phenotype (Fig. 1a, b). Moreover, the phenotypes of *AGPS* knockdown in
162 TRPA1-A/B neurons were comparable to those in *TRPA1-A/B* KO (*TRPA1-AB*$^{GAL4}$) flies (Fig. 2e,
163 f). To further confirm that thermotactic behaviors depend on *AGPS*, larvae were subjected to a
164 thermal two-choice assay (20ºC and 29ºC). The higher temperature was highly aversive for control
165 larvae, whereas reduced or no avoidance was observed in *AGPS*$^{KO}$ (Fig. 2g) or *AGPS* knockdown
166 in TRPA1-A/B neurons (Fig. 2h), respectively. Overall, these results strongly suggest that *AGPS*
167 plays a crucial role in modulating the thermosensory responses of TRPA1-A/B-expressing neurons
168 in *Drosophila*.
169 In *Drosophila melanogaster*, there are four functional TRPA1 splicing variants
170 expressed in distinct sensory neurons[30, 31] and TRPA1-A/B receptors are exclusively present in cell
171 subsets of the CNS in larvae[27]. We observed the morphology of TRPA1-A/B-expressing neurons
172 in the CNS and found no obvious structural changes with *AGPS* knock down (Supplementary Fig.
173 3). This suggested that functional reduction of *AGPS* may not alter the development and cell fate
174 of the TRPA1-A/B neurons.
175
176 ***Ether phospholipids modulate the temperature threshold for dTRPA1 activation***
177 We hypothesized that AGPS-produced ePLs influence thermosensation in larvae by directly
178 modulating thermosensory proteins such as TRPA1. To elucidate the functional role of ePLs in
179 temperature-evoked activation of TRPA1, we conducted an electrophysiological analysis using
180 cultured cells. First, we tested dTRPA1-A isoforms expressed in mammalian HEK293T cells.
181 HEK293T cells intrinsically harbor ePLs; ePEs and ePCs accounted for 4.2% ± 0.01% of total PE
182 and 15.8% ± 0.1% of total PC, respectively (Supplementary Fig. 4a–d, Supplementary Table 5, 6).
183 To deplete ePLs from cells, we generated an *AGPS* KO cell line using CRISPR-Cas9. Both ePEs
184 and ePCs were successfully depleted in the absence of functional human AGPS (Supplementary
185 Fig. 4a–d, Supplementary Table 5, 6). Next, we transiently expressed dTRPA1-A in wild type and
186 *AGPS* KO cells; there was no difference in heat-induced dTRPA1-A activation (temperature

187 threshold for activation and the current density) with presence or absence of ePLs (Supplementary
188 Fig. 4e–h). We also tested dTRPA1-A chemical responses by stimulating with an electrophilic
189 TRPA1 activator, allyl isothiocyanate (AITC). Although we observed a small increase in the
190 current density at a low AITC concentration (20 μM) in *AGPS* KO cells, such difference was not
191 observed at a saturated concentration (300 μM) (Supplementary Fig. 4i, j).

192 Since HEK293T cells were enriched in ePCs rather than ePEs, the major endogenous
193 ePLs in *Drosophila* CNS, we used S2R+ cells, a *Drosophila* embryonic cultured cell line, as they
194 lack the ability to synthesize ePLs. Accordingly, we established ePL-producing S2R+ cell lines
195 using two distinct approaches: (i) supplementation of alkylglycerol (AG) as a precursor of ePLs to
196 wild type cells to bypass the requirement of AGPS, or (ii) supplementation of fatty alcohol to cells
197 overexpressing dAGPS to drive ePL biosynthesis (Fig. 3a). The lipid analysis revealed successful
198 ePL production in S2R+ cells with both approaches (Fig. 3b–e, Supplementary Table 7, 8).
199 Importantly, the production of ePEs, but not ePCs, was primarily induced, consistent with the ePL
200 composition in larvae (Fig. 1d, e). A product ion scan analysis demonstrated that supplementation
201 with hexadecanoyl glycerol (16-AG) induced the production of ePE (32:1) and ePE (34:1),
202 considered to introduce palmitoleic acid (C16:1) and oleic acid (C18:1) at the ester-linked position,
203 respectively (Supplementary Fig. 5a, b), suggesting that a hexadecyl alcohol without double bonds
204 (O-16:0) was bound at ether-linked position. Supplementation with octadecyl alcohol (18-OH) to
205 AGPS-expressing cells resulted in the production of ePE (34:1) and ePE (36:1) containing
206 octadecyl alcohol (O-18:0) at ether-linked positions (Supplementary Fig. 5c). Thus, the
207 composition of the *sn*-1 hydrocarbon chain in ePLs appears to reflect the features of the
208 supplemented AG or fatty alcohol.

209 First, we evaluated the temperature-dependent dTRPA1-A activation using S2R+ cells
210 supplemented with 16-AG or octadecanoyl glycerol (18-AG) (Fig. 4). The average temperature
211 threshold for dTRPA1-A activation was 22.1ºC ± 0.4ºC in control S2R+ cells (Fig. 4a, d),
212 becoming significantly decreased ($p < 0.05$ in Dunnett test,) to 20.8ºC ± 0.3ºC when S2R+ cells
213 were supplemented with 18-AG (Fig. 4c, d). Although not significant ($p = 0.06$), 16-AG
214 supplementation to S2R+ cells resulted in decreasing tendency for the temperature threshold to
215 21.1ºC ± 0.3ºC (Fig. 4b, d). However, we did not observe alterations in maximum current densities
216 due to heat or AITC stimulation in ePL-producing cells (Fig. 4e–g). Consistent with the 18-AG
217 supplementation, 18-OH supplementation to AGPS-expressing S2R+ cells significant decreased

218 the temperature threshold for dTRPA1-A activation compared to control cells (20.3ºC ± 0.7ºC vs.
219 24.0ºC ± 1.2ºC; $p < 0.05$ in Student's t-test, Supplementary Fig. 6a–c). Likewise, neither heat- nor
220 AITC-evoked current densities were affected (Supplementary Fig. 6d–f). dTRPA1-B properties
221 were also tested in ePL-producing S2R+ cells. Both the temperature threshold for activation and
222 the maximum heat-evoked current densities were not altered in presence of ePLs (Supplementary
223 Fig. 7a–d). In contrast, AITC-induced current density was significantly reduced in ePL-producing
224 S2R+ cells both at low (30 μM) and high concentrations (300 μM) ($p < 0.05$ in Student's t-test,
225 Supplementary Fig. 7e, f). Taken together, these results suggest that ePLs, particularly ePEs in the
226 plasma membrane, reduce the temperature threshold for heat-evoked dTRPA1-A activation, which
227 may be important for thermosensory function in animals.
228
229 ***Mechanosensory function is regulated by ether phospholipids***
230 Difference in membrane lipid composition reportedly leads to alterations in membrane properties
231 thereby affecting the activity of mechanosensory channels[13, 14]. This evidence together with our
232 findings led us to expect that mechanosensory function could also be affected by *AGPS* mutation
233 and associated ePL loss in *Drosophila*. To investigate this point, we evaluated larval
234 mechanosensory responses. First, we assessed tactile sensation by measuring responses to a gentle
235 touch to the nose of freely moving larva; no difference in responses was observed between control
236 and $AGPS^{KO}$ larvae (Fig. 5a). Second, we characterized mechanical nociception by poking a larva
237 using von Frey filaments of three different forces (20.1, 47.0, and 70.0 mN). Nociceptive rolling
238 behavior to the weakest force (20.1 mN), but not stronger ones, was significantly decreased in
239 $AGPS^{KO}$ compared to control larvae ($p < 0.05$ in Student's t-test, Fig. 5b). We then used different
240 GAL4 lines for *AGPS* knockdown to identify the mechanosensory neurons involved in the
241 reduction in mechanical nociception. Several receptor genes have been reported as responsible for
242 the von Frey filament responses, including *PIEZO*[32], *TRPA1-C/D*[30, 33], *ppk*[34], and *painless*[35]. When
243 *AGPS* RNAi was induced using *PIEZO-GAL4* and $TRPA1\text{-}CD^{GAL4}$, a significant decrease in the
244 response to the von Frey filament (20.1 mN) was observed ($p < 0.05$ in Dunnett test) (Fig. 5c).
245 These results suggest that AGPS and its product ePL could modulate responsiveness in
246 mechanosensory neurons.
247 This result drove us to investigate whether ePLs modulate the activation of a PIEZO
248 mechanosensor. The PIEZO response to its activator Yoda1[36] was evaluated through $Ca^{2+}$ imaging

249 to test the functional role of ePLs in channel activation. PIEZO-expressing S2R+ cells were
250 stimulated with Yoda1 perfusion, which evoked a stochastic $Ca^{2+}$ increase in a small number of
251 cells (11.1% ± 3.1%; Fig. 6a, b, d, and e). When S2R+ cells were supplemented with 18-AG before
252 the experiments, Yoda1 perfusion elicited significantly higher $Ca^{2+}$ increases in a larger cell
253 population (28.7% ± 3.8%, $p < 0.01$ in Student's t-test; Fig. 6 a, c–e). These results suggested that
254 ePLs enhance PIEZO mechanosensitivity, thereby regulating animals' mechanical responses.
255 Altogether, our findings demonstrated that loss of *AGPS* and ePLs influence both thermosensory
256 and mechanosensory functions in *Drosophila*, and that ePLs play crucial roles in modulating the
257 activity of multiple sensory ion channels.
258
259 ***Ether phospholipids alter membrane tension and lipid order***
260 Previous reports have shown that lipid modulation alters membrane tension, which can impact the
261 activity of sensory channels[13, 37]. To get further insights into the effects of ePEs on membrane
262 properties in S2R+ cells, we used different approaches to quantify membrane tension and lipid
263 order.
264 First, we measured membrane tension through atomic force microscopy (AFM) force
265 curve measurement. Parts of the cell surfaces were scanned with AFM while intermittently
266 recording force curves to determine the Young's modulus, which reflects membrane tension at
267 each point (Supplementary Fig. 8a). The median value of the calculated Young's modulus in
268 control was $0.95 \times 10^5$ Pa (Fig. 7a) while that in 18-AG supplemented S2R+ cells was $2.4 \times 10^5$
269 Pa, significantly higher ($p < 0.001$, Mann–Whitney U-test) than control cells. Second, we utilized
270 a Flipper-TR probe to measure membrane tension. When the probe is incorporated into the plasma
271 membrane, the emitted fluorescent lifetime correlates with the membrane tension[38]. A longer
272 fluorescent lifetime was observed for 18-AG supplemented S2R+ cells compared to the control
273 (Fig. 7b, Supplementary Fig. 8b). These distinct measurements consistently showed an increase in
274 membrane tension in the presence of ePLs in the plasma membrane.
275 Last, we assessed the lipid order using a LipiORDER Dye[39]. A significant red shift ($p <$
276 $0.001$, Mann–Whitney U-test) in fluorescence spectrum was observed in 18-AG supplemented
277 S2R+ cells (Fig. 7c–e), suggesting that ePE-harboring membranes are in more lipid-disordered
278 states than ePE-depleted membranes. Taken together, these results demonstrate that ePEs modify
279 the physicochemical properties of the plasma membrane, which potentially leads to changes in the

activity and/or sensitivity of sensory proteins, such as TRPA1 and PIEZO. Further, the membrane properties of ePL-containing neurons may be altered as well, which could contribute to proper sensory tuning in *Drosophila*.

## DISCUSSION

In this study, we discovered a unique lipid molecule, ePLs, in neurons regulating sensory functions in *Drosophila.* ePLs have received increased attention due to their functional association with neurodegenerative diseases and metabolic disorders accompanied by systemic inflammation; potential roles such as being a scavenger of oxidative stress and a reservoir of fatty acid second messengers[40], which could modulate the function of ion channels[41], have been proposed. Recent studies have explored their involvement in ferroptosis and cancer treatment[42]. Even when ePLs are closely linked to many physiological and pathological events, the underlying mechanisms and specific targets of ePLs remain unclear. Our data demonstrate that ePLs are required for intrinsic sensory responses by modulating the responses of multiple sensory proteins, such as TRPA1 and PIEZO. The regulatory roles of ePLs on ion channel activity are open for discussion as there is a small number of studies available. Presence of PUFAs in the *sn*-2 position of glycerol backbone in ePLs and their metabolites has been discussed as direct activators of ion channels[40]. Also, the ion transport activity of sarcosomal sodium–calcium exchanger was reported to be enhanced in plasmalogen-containing proteoliposome[43]. However, there is few evidence that ePLs can modulate channel activity.

The functional correlation between ePLs and ion channels might be, at least partially, explained by the alteration of membrane properties. Previous research on mouse PIEZO1 showed that an increase in saturated FA in the cell membrane negatively regulates channel activity by bringing the membrane to an "ordered" state[13]. Since our LipiORDER analysis revealed that the membrane in ePL-lacking control S2R+ cells exhibited a much more "ordered" state than ePL-producing cells (Fig. 7e), the lower activity of *Drosophila* PIEZO1 in control cells could result in a more ordered state of the cell membrane in the absence of ePLs. In addition, our AFM and Flipper-TR imaging-based assays demonstrated that ePLs increase cell membrane tension (Fig. 7a, b). Since PIEZO1 responds to changes in cell membrane tension and deformation[44], the increased activity observed in ePL-producing S2R+ cells may be due to altered force thresholds for inducing cell membrane deformation. Regarding TRPA1, it remains unclear how the physicochemical properties of the cell membrane influence the temperature sensitivity of TRPA1 and other thermosensitive TRP channels. Previous research has shown that eicosapentaenoic acid and its derivatives modulate mammalian thermosensitive TRPV4 responses to ligands through alterations in membrane tension[37], but whether temperature TRPV4 activation is affected remains unknown.

314 As temperature affects lipid order, differences in lipid order between control and ePL-producing
315 S2R+ cells might be an underlying mechanism for the altered temperature threshold of *Drosophila*
316 TRPA1. For example, a previous report claimed that increasing unsaturated FAs in the cell
317 membrane, which should increase lipid disorder, resulted in enhanced heat responsiveness of
318 TRPA1 neurons and decreased preferred temperature of *Drosophila* larvae[19]. Further research is
319 needed to clarify the parameters of cell membrane properties involved in regulating the
320 temperature threshold of TRPA1 activation.

321 An intriguing question is whether ePLs can directly modulate channel functions through
322 direct binding to specific sites aside from altering membrane properties. Various lipid molecules
323 directly interact with TRP channels to modulate their functions[8], including temperature sensitivity.
324 For example, temperature threshold modification in mammalian TRPM8 is regulated by
325 interaction with $PIP_2$[45]. Further, TRP channels can possess a phospholipid-binding site in the S4–
326 S5 linker domain, which TRPA1 has[46]. The difference between ePLs and general phospholipids
327 lies in the type of linkage between the hydrocarbon chains at the *sn*-1 position in the glycerol
328 backbone: ether phospholipids have a (vinyl) ether linkage whereas phospholipids have an ester
329 linkage. In case of ester bonds, the oxygen molecule at the α-carbon can form hydrogen bonds and
330 affect intermolecular interactions. While the interaction at the polar head group of PL has been
331 mainly discussed in TRP channels[47], the differential interaction between ether and ester bond at
332 the *sn*-1 position of PL backbone may also be involved in the formation of lipid-TRP channel
333 interactions. Moreover, our results revealed that ePE, rather than ePC, may be crucial for
334 modulating TRPA1 function by comparing HEK293T cells (Supplementary Fig. 3) and ePL-
335 producing S2R+ cells (Fig. 3, Supplementary Fig. 6). These observations may emphasize the
336 contribution of the direct interaction between TRP channels and membrane phospholipids,
337 especially ePEs, in addition to the modification of membrane properties. For PIEZO, the
338 asymmetric distribution of PS in the lipid bilayer mostly regulates the channel[15]. Moreover, lipid
339 binding was observed in the cryo-electron microscopy structural analysis of PIEZO1 in lipid
340 nanodiscs[44]. Although the structures of PIEZO channels and all the thermosensitive TRP channels
341 including TRPA1 have been solved at an atomic level, how lipid molecules contribute to
342 mechanical or temperature activation of channels remains unclear. Future research may clarify the
343 structural and functional coupling of membrane lipids including ePLs and TRP channels.

344 This study demonstrated the expression of the ether lipid synthesis enzyme, AGPS, and
345 the presence of ether lipids in the CNS of *Drosophila*. Product ion scan analysis of major ePL
346 species in the CNS showed a prevalence of plasmanyl-type ePLs, which have no double bond,
347 rather than plasmenyl-types with a vinyl-ether bond. In humans, about 20% of ePLs are plasmenyl-
348 type plasmalogen[21]. The lipidomic analysis of honeybee (*Apis mellifera*) showed abundant non-
349 plasmenyl-type ePLs in the CNS[48], suggesting that plasmanyl-type ePLs may be prevalent in the
350 CNS of insects. To date, most discussions focus on the function of plasmenyl-type plasmalogen
351 ePLs. Particularly, on the high sensitivity of the vinyl–ether linkage with a double bond to reactive
352 oxygen species and its correlation with oxidative stress[49]. In contrast, our study clearly identified
353 the functional roles of nonplasmenyl-type ePLs on sensory channels. While the possibility of a
354 correlation between changes in cell membrane tension due to oxidative stress and the activation of
355 mechanoreceptor channels and cell death have been discussed[50], the changes in cell membrane
356 properties caused by ePLs shown in this study may be another molecular basis for the intrinsic
357 sensory regulation in cells and animals.
358 Recently, Δ1-desaturase, plasmanylethanolamine desaturase 1 (PEDS1, TMEM189),
359 has been identified as the enzyme responsible for inserting a double bond at the *sn*-1 position of
360 ePLs[51]. However, in *Drosophila*, the putative PEDS1 gene, *Kua*, does not show high expression
361 in the CNS according to FlyAtlas RNA-seq analysis[52]. This could explain the minimal presence of
362 plasmenyl-type ePLs in the CNS of *Drosophila* (Supplementary Fig. 2). It would be interesting to
363 specifically explore the expression pattern and function of Kua in *Drosophila*. In addition to the
364 CNS, ePLs are abundantly present in glial cells in mammals[53]. Since the temperature-dependent
365 motility of microglia is modulated by thermosensitive TRPV4[54] and PIEZO1 activity is reportedly
366 essential for the myelination[55], it would be interesting to test whether ePLs are involved in the
367 regulation of these channels in glial cells.
368 In conclusion, we showed that ePLs modulate distinct functions of the sensory proteins
369 such as TRPA1 and PIEZO. Since somatosensory channel proteins are involved in various
370 physiological functions.[56, 57], exploring the integrative roles of ePLs as a regulator of receptor
371 proteins may shed light on the various biological processes and diseases related to channel proteins.
372

373 **METHODS**

374 **Fly stocks and husbandry**

375 $w^{1118}$ was used as a control unless otherwise specified. The following strains were obtained from
376 Bloomington Drosophila Stock Center (BL) or Vienna Drosophila RNAi Center (VDRC): 5×*UAS-*
377 *mCD8::GFP* (BL #5137), *piezo-GAL4* (BL #59266), *painless-GAL4* (BL #27894), *UAS-dicer-2*
378 on II (VDRC #60008), *UAS-dicer-2* on III (VDRC #60009), and *UAS-AGPS* RNAi (VDRC #3321).
379 The following stocks were provided by the indicated investigators: $TRPA1\text{-}AB^{GAL4}$, $TRPA1\text{-}CD^{GAL4}$,
380 *iav-GAL4*, and *TRPL-GAL4* (C. Montell), and *ppk-GAL4* (D. N. Cox). All fly strains were
381 outcrossed to the control line ($w^{1118}$) for 4–5 generations. Flies were reared on standard cornmeal-
382 yeast medium (19 g agar, 180 g cornmeal, 100 g dry brewer's yeast Ebios, 250 g glucose, 24 mL
383 Methyl 4-hydroxybenzoate [10% w/v solution in 70% ethanol], and 8 mL propionic acid in 2500
384 mL reverse osmosis [RO] water). The flies were reared in a 25°C incubator under a 12-h light/12-
385 h dark cycle.

386

387 **Generation of AGPS knock-out flies**

388 *AGPS* knock-out ($AGPS^{KO}$) flies were generated in our laboratory using the CRISPR-Cas9 system.
389 The guide RNA sequence (5′-AATGGCAGCCAAGCGGAATG-3′) was designed using the
390 flyCRISPR target finder (http://targetfinder.flycrispr.neuro.brown.edu/) and cloned into the pU6-
391 _3-BbsI-chiRNA vector (Addgene). To achieve homologous recombination, we employed as
392 donor template the pHD-ScarlessDsRed (Drosophila Genomics Resource Center), which contains
393 1045 bp upstream and 945 bp downstream of the Cas9-mediated double-strand break site in the
394 *AGPS* genome sequence. Subsequently, the constructed vectors were injected into embryos of vas-
395 cas9 on III (BL #51324). Two distinct $AGPS^{KO}$ clones, $AGPS^{KO1}$ and $AGPS^{KO2}$, were obtained and
396 outcrossed individually to the control line ($w^{1118}$) for five generations. For all experiments,
397 $AGPS^{KO1}$ was the designated line unless otherwise specified.

398

399 **Measurement of pupariation time**

400 To enhance egg production, flies were introduced into vials containing standard food supplemented
401 with a yeast paste for ≥48 h following $CO_2$ exposure. Flies were transferred to new vials containing
402 standard food for egg laying for 3 h. These vials were placed inside a plastic bag with water supply
403 to maintain high humidity before measurements. The number of pupae on the vial wall was counted

404 during the light period, 114–192 h AEL. To determine the time at which 50% of the animals
405 underwent pupariation ($T_{50}$), we utilized the maximum number of pupae observed in each vial and
406 performed linear regression analysis on the growth curve.
407
408 **Quantitative PCR for *Drosophila* larvae and cells**
409 To prepare the whole body sample of late third instar larvae (120 h AEL), 10 larvae were collected
410 and rinsed in RO water twice. To isolate the tissues, the larvae were placed in ice-cold phosphate-
411 buffered saline (PBS), and the body wall cuticles were carefully opened using micro scissors. After
412 removing the guts and major tracheal organs, the CNS (brain and ventral nerve cord), fat body,
413 and carcass (body wall cuticles) were collected. Tissues were obtained from 5–10 larvae. Whole
414 body or tissue samples were homogenized by a pestle in Sepasol-RNA I Super G (Nacalai Tesque).
415 For culture cell samples, human embryonic kidney 293T (HEK293T) cells or *Drosophila* S2R+
416 cells were grown in 60-mm dishes at 37 or 25ºC, respectively, until reaching confluence. Then,
417 cells were washed with PBS and homogenized in Sepasol-RNA I Super G (Nacalai Tesque). Total
418 RNA was extracted following the manufacturer's protocol.
419 To isolate *ppk*-positive peripheral sensory neurons from late third instar larvae
420 expressing mCD8 in *ppk-GAL4* neurons (*UAS-mCD8::GFP*; *ppk-GAL4*), magnetic-bead-based
421 cell sorting was utilized as previously reported[58], with modifications. Fifty larvae were placed in
422 ice-cold PBS, and the posterior end was excised. The cuticle was inverted, and the internal organs
423 removed. Cuticles were then transferred into a microtube and treated with 50 µg/µL Liberase and
424 20 mU/µL DNase in 1 mL PBS supplemented with 0.02% Tween 20 (PBSTw) for 30 min at 25ºC
425 with agitation. The homogenates were filtrated through a 100 µm mesh and further filtrated
426 through a 30 µm mesh to remove debris. All apparatuses were coated with 0.1% globulin free-
427 bovine serum albumin (BSA; 016-15111, Wako). Dissociated cells were then collected by
428 centrifugation for 20 min at 300 ×*g*, and the supernatant was removed. Next, cells were
429 resuspended in PBSTw and precleared with protein G Dynabeads for 10 min at 4ºC with rotation.
430 The cell suspension was then incubated with α-CD8 antibody-coated protein G Dynabeads for 20
431 min at 4ºC with rotation. Bead-attached cells were collected using a magnetic stand and washed
432 with PBS five times. Total RNA was extracted from bead-bound cells using NucleoSpin RNA Plus
433 XS (Macherey–Nagel) following the manufacturer's protocol. The RNA concentration was
434 measured using the QuantiFluor RNA System (Promega).

435 After obtaining the total RNA, cDNA was synthesized using ReverTra Ace. The
436 expression level of the *AGPS* gene was quantified by the ΔΔCt method, using *rp49* as a reference
437 gene; KOD SYBR was used for the qPCR, which was performed on StepOne (Applied
438 Biosystems).
439
440 **Lipid analysis**
441 For *Drosophila* tissues (10 whole bodies and the CNS of late third instar larvae), lipid extraction
442 was performed using the Bligh and Dyer method[59]. Samples were homogenized in MilliQ water
443 on ice and total lipids extracted using a solvent mixture containing water/methanol/chloroform
444 (1:1:1, v/v) twice. For culture cells, total lipids were extracted using the MTBE method[60]. Cells on
445 dish were detached with PBS and collected in a microtube by centrifugation (1000x *g*, 5 min).
446 Then, cells were resuspended in 100 μL MilliQ water, and total lipids extracted using
447 MTBE/methanol/water (10:3:2.5, v/v) twice.
448 The solvent was evaporated under nitrogen gas, and the final total lipid extract
449 redissolved in methanol. Phospholipids, including ether-type phospholipids, were analyzed by LC-
450 MS/MS using LC-30AD coupled to a triple quadrupole mass spectrometer LCMS-8040
451 (Shimadzu), as previously described[19]. For multiple reaction monitoring (MRM), the transition of
452 $[M + H]^+ \rightarrow 184.0$ was used for PC and $[M + H]^+ \rightarrow [M + H]^+ - 141.1$ was used for PE. For the
453 product ion scan analysis of ePEs, $[M–H]^–$ ions were used as precursor ions derived from PE and
454 scan from m/z:350 to m/z:150.
455
456 **Temperature gradient assay**
457 The temperature gradient assay was conducted following the previously described method[61] with
458 modifications. Aluminum trays [180 mm (W) × 40 mm (D) × 5 mm (H)] were coated with 20 mL
459 of 2% agarose. The left and right ends of the tray were placed on top of two aluminum blocks
460 individually temperature-controlled using a circulating water bath. The surface temperature of the
461 agarose was monitored with a thermometer to create a thermal gradient ranging from 8 to 35ºC
462 (1.5ºC/cm).
463 Late third instar larvae (120 h AEL) were prepared in the same manner as for pupariation
464 measurements. Larvae were collected and washed twice with an 18% sucrose solution and
465 thoroughly rinsed with RO water twice. After a 10-min recovery period, 30–50 larvae were

466 released onto three agarose trays in regions where the surface temperature was approximately 28ºC.
467 Each tray was covered with a clear acrylic lid during the assay. The larvae were allowed to explore
468 the agarose under red LED light (>600 nm) in a black acrylic box. After 10 min, the distribution
469 of larvae on the agarose was captured using a digital camera. To quantify the temperature
470 distribution of larvae, the temperature at which each larva was positioned was calculated using the
471 following equation: Temperature (ºC) = Distance from the position at 8ºC (cm) × 1.5 (ºC/cm) +
472 8ºC. Larvae located within 0.5 cm from the walls or outside the tray were omitted from calculations.
473

474 **Thermal two-way choice assay**

475 The assay was conducted on an aluminum tray [90 mm (W) × 130 mm (D) × 8 mm (H)] coated
476 with 25 mL of 2% agarose. The test tray was placed on top of two adjacent aluminum blocks,
477 separated using a thin plastic film (~1 mm) as spacer. Each block was individually temperature-
478 controlled using a circulating water bath. To prevent agarose from drying, the surface was gently
479 scratched and sprayed with water. The surface temperature on each side of the test tray was
480 confirmed using a thermometer.

481 At the beginning, 40–60 larvae were released at the border between the two temperature
482 zones and allowed to explore the tray under red LED light in a black acrylic box. After 15 min, the
483 distribution of larvae on the tray was captured using a digital camera, and the number of larvae in
484 each temperature zone tabulated. The avoidance index was calculated using the following formula:
485 (Number of larvae on 20ºC − Number of larvae on 29ºC)/Total number of larvae on both sides of
486 the test tray. Larvae within the release zone (1 cm wide) were not counted in either temperature
487 zones, and those outside the trays were not included in the calculation.
488

489 **Tactile response assays**

490 Late third instar larvae were prepared as for the temperature gradient assay. The gentle-touch assay
491 was performed as described previously[62]. The anterior end of freely moving larvae was lightly
492 touched with a *Φ* 0.1mm nickel–titanium filament. Larval responses were scored as follows: 0, no
493 response; 1, hesitation; 2, turn or withdrawal of the anterior segments; 3, single reverse contraction;
494 or 4, multiple reverse contraction.

495 For the mechanical nociception assay, von Frey filaments with different forces were
496 fabricated using a nickel–titanium filament[63]. Filament forces were calibrated by measuring the

497 weight required to bend them and converting the values to force using the following equation:
498 force (mN) = weight (g) × gravity acceleration (9.8 m/s²). Larvae were released on a 60 mm dish
499 under a dissection microscope and stimulated once on the center of their body with a filament per
500 larva. The number of larvae responding to the stimuli within 5 s was recorded.
501
502 **Immunohistochemistry**
503 The CNS of late third instar larvae was dissected in a buffer containing 5 mM TES, 10 mM HEPES,
504 120 mM NaCl, 3 mM KCl, 4 mM $MgCl_2$, 2 mM $CaCl_2$, 10 mM $NaHCO_3$, 10 mM trehalose, 10
505 mM glucose, and 10 mM sucrose (pH 7.25). The dissected CNS was then placed on 12mm $\phi$ cover
506 glass (C012001, Matsunami) coated with poly-L-lysine and fixed with 4% paraformaldehyde and
507 0.4% Triton-X100 for 30 min at room temperature. Subsequently, samples were washed with PBS
508 containing 0.3% Triton X100 (PBSTx) and blocked with 5% normal goat serum (NGS) in PBSTx
509 for 30 min at room temperature. Then, samples were incubated with an α-GFP primary antibody
510 (1:500; #A6455, Invitrogen) in 5% NGS/PBSTx overnight at 4ºC, followed by washing with
511 PBSTx. Next, samples were incubated with the secondary antibody (α-Rabbit IgG-Alexa488,
512 1:1000; #A11034, Invitrogen) in PBSTx for 3 h at 4ºC and washed with PBSTx. Finally, samples
513 were mounted on a glass slide using Fluoromount (Diagnostic BioSystems). Fluorescence was
514 captured using an Olympus FV1200 IX83 confocal microscope equipped with a 30×/1.05 objective
515 lens.
516
517 **HEK293T cell culture, transfection, and generation of *AGPS* KO cells**
518 Cells were cultured in Dulbecco's modified Eagle Medium supplemented with 10% fetal bovine
519 serum (#10437-028, Gibco), 1× GlutaMAX, and 50 mg/mL penicillin/50 units/mL streptomycin
520 at 37ºC in 5% $CO_2$.
521 The CRISPR-Cas9 system[64] was employed to establish *AGPS* KO HEK293T cells. The
522 guide RNA sequence (5′-CAATTTGACAGCTCATGTAG-3′) was designed using CRISPick
523 (https://portals.broadinstitute.org/gppx/crispick/public) and cloned into the pSpCas9 (BB)-2APuro
524 (PX459) vector (Addgene). The plasmid was transfected into cells using lipofectamine 2000 and
525 Plus reagent (Invitrogen) and incubated for 6 h at 37ºC. After changing to standard medium, cells
526 were incubated for 2 days, followed by treatment with 10 µg/mL puromycin. Puromycin-resistant
527 colonies were collected, and successful genome editing was confirmed in each colony using the

528 T7-endonucrease assay[64]. Cells from positive colonies were isolated as individual clones by
529 limiting dilution in a 96-well plate (0.5 cell/well). Nonhomologous end joining at the designated
530 region in the clones was confirmed by genome sequencing. *AGPS* KO cells were maintained with
531 standard medium, supplemented with 10 μg/mL puromycin.
532 For the functional dTRPA1-A assay, 1 μg dTRPA1-A in pcDNA3.1(+) vector and 0.1 μg
533 pCMV-DsRed vector were co-transfected into control or *AGPS* KO cells ($2 \times 10^5$ cells in a 35-mm
534 dish) using lipofectamine 2000 reagent and Plus reagent (Invitrogen) dissolved in 1X OPTI-MEM
535 I medium, following the manufacturer's protocol. After incubating 3–4 h in a 37ºC incubator, the
536 cells were reseeded on 12-mm cover slips (Matsunami) in a 60-mm dish and further incubated
537 overnight at 33ºC in 5% $CO_2$.
538
539 **S2R+ cell culture, transfection, and generation of stable cell lines**
540 Cells were cultured in Schneider's *Drosophila* medium (Gibco) supplemented with 10% fetal
541 bovine serum (#10437-028, Gibco), and 50 mg/mL penicillin/50 units/mL streptomycin at 25ºC.
542 For the lipid supplementation experiment, 1 mM lipids were mixed and sonicated in 10
543 mg/mL fatty-acid free BSA/0.9% NaCl solution for 15 min to form a complex. As negative control,
544 the same volume of solvent (ethanol) was mixed with a BSA/NaCl solution. The lipid-BSA
545 complex was diluted in the culture medium to achieve a final concentration of 100 μM lipids and
546 incubated with the cells for 24 h. The following lipids were purchased: 1-O-Hexadecyl-rac-
547 glycerol (16-AG; #sc-205917, Santa Cruz), Glycerol 1-Oleyl Ether (18-AG; #G598710, Tront
548 Research chemicals), and 1-Octadecanol (18-OH; #O0006, Tokyo Chemical Industry).
549 For the functional assay of dTRPA1-A and dTRPA1-B, we established stable cell lines
550 expressing each isoform. dTRPA1-A or dTRPA1-B in pMT vectors were co-transfected with pBS-
551 puro using X-tremeGENE 9 DNA transfection reagent (Roche), and stable cells were selected and
552 maintained in the presence of 10 μg/mL puromycin. Metallothionein promoter-dependent dTRPA1
553 expression was induced by supplementing cells with 500 μM $CuSO_4$ for 24 h. For the functional
554 assay of dTRPA1-A in dAGPS-expressing cells, a cloned cell line stably expressing dAGPS was
555 established. The dAGPS in the pAc5.1-V5-His vector was co-transfected with pBS-puro using the
556 X-tremeGENE 9 DNA transfection reagent. Cells expressing N-term-V5-His-dAGPS were
557 selected in the presence of 10 μg/mL puromycin, and a monoclonal cell line was established using
558 limiting dilution in a 96-well plate (0.5 cell/well). pAc5.1-dTRPA1-A and pAc5.1-EGFP were

559 transiently co-transfected into control or dAGPS stable cells using TransFectin Lipid Reagent
560 (BioRad). After a 24 h incubation, transfection medium was removed and replaced by growth
561 medium, and incubated for another 24 h at 25ºC For the functional assay of dPIEZO, pAc5.1-
562 dPIEZO and pAc5.1-DsRed were transiently co-transfected into control cells using TransFectin
563 Lipid Reagent, as described above.
564
565 **Electrophysiology**
566 For whole-cell patch-clamp recordings, the extracellular bath solution contained 140 mM NaCl, 5
567 mM KCl, 2 mM $MgCl_2$, 2 mM $CaCl_2$, 10 mM HEPES, and 10 mM glucose (pH 7.4 for HEK293T
568 cells and pH 7.2 for S2R+ cells, adjusted with NaOH). The pipette solution for HEK293T cells
569 contained 140 mM KCl, 5 mM EGTA, and 10 mM HEPES (pH 7.4, adjusted with KOH). The
570 pipette solution for S2R+ cells contained 140 mM Cs-Aspartate, 2 mM $MgCl_2$, 0.01 mM $CaCl_2$,
571 1 mM EGTA, and 10 mM HEPES (pH 7.2, adjusted with CsOH). Voltage-clamp recordings were
572 used as described previously[65], with an Axon 200B (Molecular Devices) amplifier and pCLAMP
573 software (version 10.7; Axon Instruments). The membrane potential was held at −60 mV, and
574 experiments were performed at 25ºC. For heat stimulation of TRPA1, the temperature of the bath
575 solution was initially decreased by perfusing a precooled solution (10ºC), then increased by
576 perfusing a prewarmed solution (65ºC). The temperature of the solution near the recorded cell was
577 monitored using a TA-29 thermistor (Warner instrument).
578 The temperature threshold for dTRPA1 activation was determined in Arrhenius plots of
579 whole-cell voltage-clamp recordings using Origin software (OriginLab), as previously described[65].
580 Log scales of currents were plotted against the reciprocal of the absolute temperature (T). The
581 crossing point of the two fitted lines at which the slope changed in Arrhenius plots was defined as
582 the temperature threshold.
583
584 **Calcium imaging**
585 Cells transiently expressing dPIEZO were loaded with 5 μM Fura 2-AM (Dojindo), 0.02%
586 Pluronic F127, and 500 μM probenecid by incubation in standard culture medium for 60 min at
587 25ºC. The same bath solution for electrophysiological experiments was used for measurements.
588 Fura-2 in cells was excited at 340 and 380 nm, and the emission at 510 nm was monitored with a
589 sCMOS camera (Zyla 4.2 Plus, Andor Technology). Time-lapse images were recorded every 3 s.

590 To activate dPIEZO, 10 μM Yoda1 (TOCRIS) was applied by perfusion. The perfusion flow rate
591 was set at 4 mL/min. Ionomycin (5 μM) was applied at the end of the protocol to calibrate the
592 maximum capacity of $Ca^{2+}$ intake. Data were measured and analyzed using the iQ2 software
593 (Andor Technology), and the ratio (340/380) was calculated with Fiji software[66].
594
595 **Force curve measurement using high-speed AFM**
596 S2R+ cells, with/without 24-h supplementation with 100 μM 18-AG, were used for analysis. The
597 cells were attached on concanavalin A (Nacalai)-coated cover glass for 30 min at room temperature
598 immediately before the experiment. The force curve measurement was performed in the same bath
599 solution used for electrophysiological experiments but supplemented with 0.01% BSA. The AFM
600 used was a tip-scan high-speed AFM (TS-HS-AFM) combined with an optical microscope[67].
601 Optical images were used to confirm cell position and the positions of stiffness measurements. The
602 cantilevers used were Olympus AC10 cantilevers (length 9 μm, width 2 μm, height 0.13 μm), with
603 a carbon tip grown by electron beam deposition (EBD) at its very end. For these measurements,
604 long EBD tips were used, as they are reportedly beneficial for cell measurements[68]. Using the
605 thermal sweep method[69], the cantilevers' spring constants were determined as $0.093 \pm 0.038$ $Nm^{-1}$,
606 their resonance frequency as $433 \pm 55$ kHz, and their Q-factor as $1.34 \pm 0.09$ (averages and
607 standard deviations of 6 cantilevers). Before measuring the cells, the cantilever's sensitivity was
608 determined by performing a force map of 50 × 50 curves on a glass substrate and calculating
609 determining the slope of the force curves by a linear fit. The resulting 2500 slopes were then plotted
610 as a histogram and fitted with a Gaussian. The sensitivity was designated as the location of the
611 Gaussian's maximum. For all measurements, the scan size was 1 μm × 1 μm, and the pixel
612 resolution set to either 150 × 150 or 200 × 200 pixels.
613 To measure the mechanical properties of S2R+ cells, the edge of a cell was first located
614 in standard tapping mode with a frame time of 5–10 s. After the cell edge was reached, force curves
615 were recorded with a grid of 50 × 50 curves in between topography lines. This force mapping
616 procedure was based on inline force curve measurements[70]. Simultaneously, optical microscopy
617 images were acquired to assign each force map to a cell position. The frame time during force
618 mapping was 30–35 s. Force curves were recorded with a frequency of 1 kHz. The maximum force
619 was not controlled but was typically <500 pN. Only the flat outer regions of cells were measured
620 because the region close to the nucleus exhibited a steep upward slope that prevented stable

621 scanning conditions. Similarly, it was not possible to scan stably directly on top of the nucleus due
622 to part of the cells fluctuating and being deformed by the small lateral scanning forces.
623 The acquired force curves were fitted with the Hertz contact mechanics model assuming
624 a tip radius of 5 nm. Force curves were automatically analyzed using home-made software based
625 on IgorPro. Before fitting the force curve with the Hertz model, the linear background was
626 subtracted from the force curves to level the curves.
627
628 **Imaging-based membrane property measurement**
629 S2R+ cells, with/without 24-h supplementation of 100 μM 18-AG, were used for analysis. Cells
630 were plated on a noncoat glass bottom dish (35mm $\phi$, No.1S, D11530H, Matsunami) and
631 incubated for 24 h. Subsequently, the cells on the glass were washed with the same bath solution
632 used for electrophysiological experiments and incubated with either 2 μM Flipper-TR
633 (Spirochrome) or 100 nM LipiORDER (Funakoshi) in the bath solution for 15 min at room
634 temperature. Images were captured using a Leica TCS SP8 FALCON confocal microscope
635 equipped with a HC PL APO CS2 100×/1.40 OIL immersion objective lens, a pulsed
636 supercontinuum white light laser and HyD-SMD photon counting detectors. Images were acquired
637 at 256 × 256 pixels using 3× zoom. For Flipper-TR measurements, we performed excitation at 488
638 nm and emission at 550–650 nm. The fluorescence lifetimes were calculated from decay curves
639 using Leica LAS X Single Molecule Detection software. The fitting model was an n-exponential
640 reconvolution with instrument response function and two exponential components were estimated.
641 The longer decay time was used for subsequent analysis. For LipiORDER measurement, cells were
642 excited at 405 nm, and the emission spectrum was measured from 450 nm to 650 nm with a 25-
643 nm interval. The red to green ratio (R/G ratio) was calculated by dividing fluorescence intensities
644 at 550–650 nm by those at 450–550 nm. The optical section was set at 80 nm and 50 nm for
645 Flipper-TR and LipiORDER, respectively.
646
647 **Statistical analysis**
648 Data are presented as means ± SEMs. The times each experiment was performed (n) is indicated
649 either in figure legends or panels. To compare two samples, unpaired, two-tailed Student's *t* tests
650 were performed. To performed multiple comparison, Tukey's test or Dunnett test was used. For
651 comparison of temperature preference behavioral experiment and membrane property assay,

nonparametric Mann–Whitney's U-test (for two samples) and Kruskal–Wallis tests followed by Steel's tests (for multiple comparisons vs. control) were performed. All statistical analyses were conducted using Prism 10 (GraphPad) or JMP 14.2 software (SAS Institute). A p-value of less than 0.05 was considered statistically significant.

**ACKNOWLEDGMENT**

The fly stocks used in this study were obtained from the Bloomington Drosophila Stock Center, and NIG-FLY Stock Center. We thank Dr. Shoma Sato, Naomi Fukuta, Terumi Hashimoto, and Dr. Jing Lei (ExCELLS/NIPS) for supporting fly maintenance and molecular cloning experiments. We appreciate Dr. Masato Umeda (HoloBio Inc.), Dr. Akifumi Shiomi (RIKEN), and Dr. Akira Murakami (University of Shizuoka) for giving us the kind advises to the project.

**FUNDING**

This work was supported by Grant-in-aid for Scientific research 19K23790 and 21K15192 (for T. Suito), 21H02531 (for T. Sokabe), and 22H04926 (for T.N.) from Japan Society for the Promotion of Science (JSPS) and Ministry of Education, Culture, Sports, Science and Technology, Grant-in-Aid for Transformative Research Areas — Platforms for Advanced Technologies and Research Resources "Advanced Bioimaging Support" JP22H04926 (for T. Sokabe) from JSPS, and the Japan Agency for Medical Research and Development (AMED)-PRIME 23gm6510014h0002 (for T. Sokabe) from AMED.

**AUTHORS CONTRIBUTION**

T. Suito contributed to designing, conducting, and analyzing most of the experiments, preparing the draft and the final version of manuscript. T. Sokabe contributed to supervising the project, preparing the draft and the final version of manuscript. M. Tominaga contributed to supervising the project. K.N. contributed to supervising and performing the LC-MS lipid analysis. X. D. contributed to performing fly behavioral experiments. C.G. and T.U. contributed to supervising and conducting the force curve measurement using AFM. M. Tsutsumi and T.N. contributed to supervising chemical probe-based membrane property measurement. Y.H. contributed to dPIEZO cloning and supervising the calcium measurement experiment.

## COMPETING INTERESTS

The authors declare that they have no conflicts of interest with the contents of this article.

687 **REFERENCES**


688 1. Caterina MJ, Schumacher MA, Tominaga M, Rosen TA, Levine JD, Julius D. The
689 capsaicin receptor: a heat-activated ion channel in the pain pathway. *Nature* **389**, 816-824
690 (1997).
691 2. Dhaka A, Murray AN, Mathur J, Earley TJ, Petrus MJ, Patapoutian A. TRPM8 is required
692 for cold sensation in mice. *Neuron* **54**, 371-378 (2007).
693 3. Moqrich A*, et al.* Impaired thermosensation in mice lacking TRPV3, a heat and camphor
694 sensor in the skin. *Science* **307**, 1468-1472 (2005).
695 4. Coste B*, et al.* Piezo1 and Piezo2 are essential components of distinct mechanically
696 activated cation channels. *Science* **330**, 55-60 (2010).
697 5. Tominaga M*, et al.* The cloned capsaicin receptor integrates multiple pain-producing
698 stimuli. *Neuron* **21**, 531-543 (1998).
699 6. Ranade SS*, et al.* Piezo2 is the major transducer of mechanical forces for touch sensation
700 in mice. *Nature* **516**, 121-125 (2014).
701 7. Kashio M, Tominaga M. TRP channels in thermosensation. *Curr Opin Neurobiol* **75**,
702 102591 (2022).
703 8. Ciardo MG, Ferrer-Montiel A. Lipids as central modulators of sensory TRP channels.
704 *Biochim Biophys Acta Biomembr* **1859**, 1615-1628 (2017).
705 9. Bradshaw HB, Raboune S, Hollis JL. Opportunistic activation of TRP receptors by
706 endogenous lipids: exploiting lipidomics to understand TRP receptor cellular
707 communication. *Life Sci* **92**, 404-409 (2013).
708 10. Sisignano M, Bennett DL, Geisslinger G, Scholich K. TRP-channels as key integrators of
709 lipid pathways in nociceptive neurons. *Prog Lipid Res* **53**, 93-107 (2014).
710 11. Taberner FJ, Fernandez-Ballester G, Fernandez-Carvajal A, Ferrer-Montiel A. TRP
711 channels interaction with lipids and its implications in disease. *Biochim Biophys Acta*
712 **1848**, 1818-1827 (2015).
713 12. Cordero-Morales JF, Vasquez V. How lipids contribute to ion channel function, a fat
714 perspective on direct and indirect interactions. *Curr Opin Struct Biol* **51**, 92-98 (2018).
715 13. Romero LO*, et al.* Dietary fatty acids fine-tune Piezo1 mechanical response. *Nat*
716 *Commun* **10**, 1200 (2019).
717 14. Romero LO*, et al.* Linoleic acid improves PIEZO2 dysfunction in a mouse model of
718 Angelman Syndrome. *Nat Commun* **14**, 1167 (2023).

719 15. Tsuchiya M*, et al.* Cell surface flip-flop of phosphatidylserine is critical for PIEZO1-
720 mediated myotube formation. *Nat Commun* **9**, 2049 (2018).
721 16. Bazinet RP, Laye S. Polyunsaturated fatty acids and their metabolites in brain function
722 and disease. *Nat Rev Neurosci* **15**, 771-785 (2014).
723 17. Custers, Emma EM, Kiliaan, Amanda J. Dietary lipids from body to brain. *Prog Lipid*
724 *Res* **85**, 101144 (2022).
725 18. Vasquez V, Krieg M, Lockhead D, Goodman MB. Phospholipids that contain
726 polyunsaturated fatty acids enhance neuronal cell mechanics and touch sensation. *Cell*
727 *Rep* **6**, 70-80 (2014).
728 19. Suito T, Nagao K, Takeuchi K, Juni N, Hara Y, Umeda M. Functional expression of
729 Delta12 fatty acid desaturase modulates thermoregulatory behaviour in Drosophila. *Sci*
730 *Rep* **10**, 11798 (2020).
731 20. Snyder F. The ether lipid trail: a historical perspective. *Biochim Biophys Acta* **1436**, 265-
732 278 (1999).
733 21. Braverman NE, Moser AB. Functions of plasmalogen lipids in health and disease.
734 *Biochim Biophys Acta* **1822**, 1442-1452 (2012).
735 22. de Vet EC, Ijlst L, Oostheim W, Wanders RJ, van den Bosch H. Alkyl-
736 dihydroxyacetonephosphate synthase. Fate in peroxisome biogenesis disorders and
737 identification of the point mutation underlying a single enzyme deficiency. *J Biol Chem*
738 **273**, 10296-10301 (1998).
739 23. Dorninger F, Forss-Petter S, Berger J. From peroxisomal disorders to common
740 neurodegenerative diseases - the role of ether phospholipids in the nervous system. *FEBS*
741 *Lett* **591**, 2761-2788 (2017).
742 24. Razeto A*, et al.* The Crucial Step in Ether Phospholipid Biosynthesis: Structural Basis of
743 a Noncanonical Reaction Associated with a Peroxisomal Disorder. *Structure* **15**, 683-692
744 (2007).
745 25. Im SH, Galko MJ. Pokes, sunburn, and hot sauce: Drosophila as an emerging model for
746 the biology of nociception. *Dev Dyn* **241**, 16-26 (2012).
747 26. Shiomi A*, et al.* Extreme deformability of insect cell membranes is governed by
748 phospholipid scrambling. *Cell Rep* **35**, 109219 (2021).
749 27. Luo J, Shen WL, Montell C. TRPA1 mediates sensation of the rate of temperature change
750 in Drosophila larvae. *Nature neuroscience* **20**, 34-41 (2017).

751 28. Rosenzweig M, Kang K, Garrity PA. Distinct TRP channels are required for warm and
752 cool avoidance in Drosophila melanogaster. *Proc Natl Acad Sci U S A* **105**, 14668-14673
753 (2008).
754 29. Kwon Y, Shen WL, Shim HS, Montell C. Fine thermotactic discrimination between the
755 optimal and slightly cooler temperatures via a TRPV channel in chordotonal neurons. *J*
756 *Neurosci* **30**, 10465-10471 (2010).
757 30. Zhong L*, et al.* Thermosensory and nonthermosensory isoforms of Drosophila
758 melanogaster TRPA1 reveal heat-sensor domains of a thermoTRP Channel. *Cell Rep* **1**,
759 43-55 (2012).
760 31. Gu P*, et al.* Polymodal Nociception in Drosophila Requires Alternative Splicing of
761 TrpA1. *Curr Biol* **29**, 3961-3973 e3966 (2019).
762 32. Kim SE, Coste B, Chadha A, Cook B, Patapoutian A. The role of Drosophila Piezo in
763 mechanical nociception. *Nature* **483**, 209-212 (2012).
764 33. Gong J*, et al.* Shear stress activates nociceptors to drive Drosophila mechanical
765 nociception. *Neuron* **110**, 3727-3742 e3728 (2022).
766 34. Zhong L, Hwang RY, Tracey WD. Pickpocket is a DEG/ENaC protein required for
767 mechanical nociception in Drosophila larvae. *Curr Biol* **20**, 429-434 (2010).
768 35. Tracey WD, Jr., Wilson RI, Laurent G, Benzer S. painless, a Drosophila gene essential for
769 nociception. *Cell* **113**, 261-273 (2003).
770 36. Syeda R*, et al.* Chemical activation of the mechanotransduction channel Piezo1. *Elife* **4**,
771 (2015).
772 37. Caires R*, et al.* Omega-3 Fatty Acids Modulate TRPV4 Function through Plasma
773 Membrane Remodeling. *Cell Rep* **21**, 246-258 (2017).
774 38. Colom A*, et al.* A fluorescent membrane tension probe. *Nat Chem* **10**, 1118-1125 (2018).
775 39. Valanciunaite J*, et al.* Polarity Mapping of Cells and Embryos by Improved Fluorescent
776 Solvatochromic Pyrene Probe. *Anal Chem* **92**, 6512-6520 (2020).
777 40. Astudillo AM, Balboa MA, Balsinde J. Compartmentalized regulation of lipid signaling
778 in oxidative stress and inflammation: Plasmalogens, oxidized lipids and ferroptosis as
779 new paradigms of bioactive lipid research. *Prog Lipid Res* **89**, 101207 (2023).
780 41. Fontaine D*, et al.* Roles of endogenous ether lipids and associated PUFAs in the
781 regulation of ion channels and their relevance for disease. *J Lipid Res* **61**, 840-858
782 (2020).

783 42. Zou Y, *et al.* Plasticity of ether lipids promotes ferroptosis susceptibility and evasion.
784 *Nature* **585**, 603-608 (2020).
785 43. Ford DA, Hale CC. Plasmalogen and anionic phospholipid dependence of the cardiac
786 sarcolemmal sodium-calcium exchanger. *FEBS Lett* **394**, 99-102 (1996).
787 44. Yang X, Lin C, Chen X, Li S, Li X, Xiao B. Structure deformation and curvature sensing
788 of PIEZO1 in lipid membranes. *Nature* **604**, 377-383 (2022).
789 45. Fujita F, Uchida K, Takaishi M, Sokabe T, Tominaga M. Ambient temperature affects the
790 temperature threshold for TRPM8 activation through interaction of phosphatidylinositol
791 4,5-bisphosphate. *J Neurosci* **33**, 6154-6159 (2013).
792 46. Suo Y, *et al.* Structural Insights into Electrophile Irritant Sensing by the Human TRPA1
793 Channel. *Neuron* **105**, 882-894 e885 (2020).
794 47. Poveda JA, *et al.* Lipid modulation of ion channels through specific binding sites.
795 *Biochim Biophys Acta* **1838**, 1560-1567 (2014).
796 48. Morfin N, Fillier TA, Pham TH, Goodwin PH, Thomas RH, Guzman-Novoa E. First
797 insights into the honey bee (Apis mellifera) brain lipidome and its neonicotinoid-induced
798 alterations associated with reduced self-grooming behavior. *J Adv Res* **37**, 75-89 (2022).
799 49. Wynalda KM, Murphy RC. Low-concentration ozone reacts with plasmalogen
800 glycerophosphoethanolamine lipids in lung surfactant. *Chem Res Toxicol* **23**, 108-117
801 (2010).
802 50. Hirata Y, *et al.* Lipid peroxidation increases membrane tension, Piezo1 gating, and cation
803 permeability to execute ferroptosis. *Curr Biol* **33**, 1282-1294 e1285 (2023).
804 51. Werner ER, *et al.* The TMEM189 gene encodes plasmanylethanolamine desaturase which
805 introduces the characteristic vinyl ether double bond into plasmalogens. *Proc Natl Acad*
806 *Sci U S A* **117**, 7792-7798 (2020).
807 52. Chintapalli VR, Wang J, Dow JAT. Using FlyAtlas to identify better Drosophila
808 melanogaster models of human disease. *Nature Genetics* **39**, 715-720 (2007).
809 53. Barnes-Velez JA, Aksoy Yasar FB, Hu J. Myelin lipid metabolism and its role in
810 myelination and myelin maintenance. *Innovation (Camb)* **4**, 100360 (2023).
811 54. Nishimoto R, *et al.* Thermosensitive TRPV4 channels mediate temperature-dependent
812 microglia movement. *Proc Natl Acad Sci U S A* **118**, (2021).
813 55. Acheta J, *et al.* Piezo channels contribute to the regulation of myelination in Schwann
814 cells. *Glia* **70**, 2276-2289 (2022).

815 56. Zhang M, Ma Y, Ye X, Zhang N, Pan L, Wang B. TRP (transient receptor potential) ion
816 channel family: structures, biological functions and therapeutic interventions for diseases.
817 *Signal Transduct Target Ther* **8**, 261 (2023).
818 57. Delmas P, Parpaite T, Coste B. PIEZO channels and newcomers in the mammalian
819 mechanosensitive ion channel family. *Neuron* **110**, 2713-2727 (2022).
820 58. Turner HN*, et al.* The TRP Channels Pkd2, NompC, and Trpm Act in Cold-Sensing
821 Neurons to Mediate Unique Aversive Behaviors to Noxious Cold in Drosophila. *Curr*
822 *Biol* **26**, 3116-3128 (2016).
823 59. Bligh EG, Dyer WJ. A rapid method of total lipid extraction and purification. *Can J*
824 *Biochem Physiol* **37**, 911-917 (1959).
825 60. Matyash V, Liebisch G, Kurzchalia TV, Shevchenko A, Schwudke D. Lipid extraction by
826 methyl-tert-butyl ether for high-throughput lipidomics. *J Lipid Res* **49**, 1137-1146 (2008).
827 61. Sokabe T, Chen HC, Luo J, Montell C. A Switch in Thermal Preference in Drosophila
828 Larvae Depends on Multiple Rhodopsins. *Cell Rep* **17**, 336-344 (2016).
829 62. Kernan M, Cowan D, Zuker C. Genetic dissection of mechanosensory transduction:
830 mechanoreception-defective mutations of Drosophila. *Neuron* **12**, 1195-1206 (1994).
831 63. Lopez-Bellido R, Galko MJ. An Improved Assay and Tools for Measuring Mechanical
832 Nociception in Drosophila Larvae. *J Vis Exp*, (2020).
833 64. Ran FA, Hsu PD, Wright J, Agarwala V, Scott DA, Zhang F. Genome engineering using
834 the CRISPR-Cas9 system. *Nat Protoc* **8**, 2281-2308 (2013).
835 65. Nguyen THD*, et al.* Single amino acids set apparent temperature thresholds for heat-
836 evoked activation of mosquito transient receptor potential channel TRPA1. *J Biol Chem*
837 **298**, 102271 (2022).
838 66. Schindelin J*, et al.* Fiji: an open-source platform for biological-image analysis. *Nat*
839 *Methods* **9**, 676-682 (2012).
840 67. Fukuda S*, et al.* High-speed atomic force microscope combined with single-molecule
841 fluorescence microscope. *Rev Sci Instrum* **84**, 073706 (2013).
842 68. Shibata M, Uchihashi T, Ando T, Yasuda R. Long-tip high-speed atomic force
843 microscopy for nanometer-scale imaging in live cells. *Sci Rep* **5**, 8724 (2015).
844 69. Hutter JL, Bechhoefer J. Calibration of atomic-force microscope tips. *Review of Scientific*
845 *Instruments* **64**, 1868-1873 (1993).
846 70. Ganser C, Uchihashi T. Microtubule self-healing and defect creation investigated by in-

line force measurements during high-speed atomic force microscopy imaging. *Nanoscale* **11**, 125-135 (2018).

851 **FIGURE LEGENDS**

852 **Fig. 1 Ether phospholipid enrichment in *Drosophila* neurons.**

853 **a** Relative *AGPS* expression level in different tissues in $w^{1118}$ third instar larvae (n = 3). CNS:
854 central nervous system. *p < 0.05, Tukey's test. **b** Relative *AGPS* expression level in *ppk*-positive
855 peripheral neurons (bead bound) and other cells (bead unbound) (n = 4). ** p < 0.01, Student's t-
856 test. **c** Total ePE area (% of total PE in whole body and the CNS) of third instar larvae (n = 4) in
857 $w^{1118}$ (control), heterozygous *AGPS* knockout ($AGPS^{KO/+}$), and homozygous *AGPS* knockout
858 ($AGPS^{KO/KO}$) are shown. *** p < 0.001, Student's t-test. Each point in **a**–**c** represents a biological
859 replicate. Data are presented as mean ± SEM. **d, e** Colormap for the composition of PE (**d**) and PC
860 (**e**) species (area% of total species) in the CNS of $w^{1118}$ (control) and homozygous $AGPS^{KO}$ third
861 instar larvae (n = 4). Phospholipid molecules are listed as PE (X:Y) or PC (X:Y), where X denotes
862 the total number of carbon molecules in acyl chains and Y the total of double bonds in acyl chains.
863 Cross marks indicate phospholipid species under detectable levels. Source data are provided as a
864 Source Data file.

865

866 **Fig. 2 AGPS regulates TRPA1-A/B-dependent thermosensation.**

867 **a**, **b** Temperature preference assay on a linear gradient for late third instar larvae of $w^{1118}$ (control,
868 n = 16), heterozygous $AGPS^{KO}$ ($AGPS^{KO1/+}$, n = 6), homozygous $AGPS^{KO}$ clones ($AGPS^{KO1/KO1}$
869 and $AGPS^{KO2/KO2}$, n = 9). **c**, **d** Temperature preference assay for late third instar larvae of control
870 (*UAS-AGPS RNAi*/+, n = 13), and *AGPS* knockdown by $TRPA1\text{-}AB^{GAL4}$ (*UAS-dicer-2/UAS-AGPS*
871 RNAi;$TRPA1\text{-}AB^{GAL4}$/+, n = 8), $TRPA1\text{-}CD^{GAL4}$ (*dicer-2/AGPS* RNAi;$TRPA1\text{-}CD^{GAL4}$/+, n = 8),
872 *TRPL-GAL4* (*UAS-dicer-2/UAS-AGPS* RNAi;*TRPL-GAL4*/+, n = 8), and *Iav-GAL4* (*UAS-dicer-*
873 *2/UAS-AGPS* RNAi;*Iav-GAL4*/+, n = 9). **e**, **f** Temperature preference assay for late third instar
874 larvae of control (*UAS-dicer-2/+*;$TRPA1\text{-}AB^{GAL4}$/+, n = 9), *AGPS* knockdown by $TRPA1\text{-}AB^{GAL4}$
875 (*UAS-dicer-2/UAS-AGPS* RNAi;$TRPA1\text{-}AB^{GAL4}$/+, n = 12), and *TRPA1-AB* knockout ($TRPA1\text{-}$
876 $AB^{GAL4}/TRPA1\text{-}AB^{GAL4}$, n = 9). Distribution of third instar larvae on a thermal gradient of 8ºC–
877 35ºC (**a, c, e**) and fraction of larvae distributed over 25ºC zones (**b, d, f**). **g, h** Avoidance index on
878 the thermal two-way choice assay at 29 vs. 20ºC of $w^{1118}$ (control, n = 7) and $AGPS^{KO}$ (n = 6) (**g**),
879 or control ($TRPA1\text{-}AB^{GAL4}$/+, n = 6) and *AGPS* knockdown by $TRPA1\text{-}AB^{GAL4}$ (*UAS-dicer-2/UAS-*
880 *AGPS* RNAi;$TRPA1\text{-}AB^{GAL4}$/+, n = 6) (**h**). Each point represents a biological replicate. Data are
881 presented as mean ± SEM. *p < 0.05; *** p < 0.001 for Mann–Whitney's U-test or Steel's test (vs.

882 control). Source data are provided as a Source Data file.

883

884 **Fig. 3 Establishment of ePL-producing S2R+ cells.**

885 **a** Synthesis pathways of ePLs. Two strategies to increase ePL production in *Drosophila* are shown.
886 (i) Supplementation with 16-AG or 18-AG (1-alkylglycerol) or (ii) *AGPS* overexpression with 18-
887 OH (fatty alcohol) supplementation. FA-CoA, Fatty acyl-CoA; DHAP, dihydroxyacetone
888 phosphate; GNPAT, dihydroxyacetone phosphate acyltransferase; MGAT, monoacylglycerol
889 acyltransferase; CDP, cytidine diphosphate; CPT, choline phosphotransferase; and CEPT,
890 choline/ethanolamine phosphotransferase. **b–e** Lipid composition in control and ePL-producing
891 S2R+ cells (n = 4) for total ePE area% of total PE (**b**), total ePC area% of total PC (**c**), and colormap
892 for composition of PE (**d**) and PC (**e**) species (area% of total PE or PC) in control cells
893 (Control/S2R+), 100 μM 16-AG supplemented cells (16-AG/S2R+), *dAGPS*-expressing cells
894 (Control/S2R+ dAGPS), and 100 μM 18-OH supplemented *dAGPS*-expressing cells (18-
895 OH/S2R+ dAGPS). Phospholipid molecules are listed as PE (X:Y) or PC (X:Y), where X denotes
896 the total number of acyl chains and Y the total of double bonds in acyl chains. Cross marks in (**d,**
897 **e**) indicate phospholipid species under detectable levels. Each point represents a biological
898 replicate. Data are presented as mean ± SEM. Source data are provided as a Source Data file.

899

900 **Fig. 4 ePLs modulates the temperature threshold for dTRPA1-A activation.**

901 **a–c** Whole-cell patch-clamp recording of dTRPA1 activation with temperature stimulation in
902 dTRPA1 expressing S2R+ cells (**a**), dTRPA1 expressing cells supplemented with 100 μM 16-AG
903 (**b**), and dTRPA1 expressing cells supplemented with 100 μM 18-AG (**c**). Left, representative
904 traces of recordings; right, Arrhenius plots from the traces in the left panels. Temperature
905 thresholds were determined as a crossing point of two fitted lines. **d–g** Quantification of the
906 temperature threshold (**d**) and peak current densities of heat (**e**), 30 μM AITC (**f**), and 300 μM
907 AITC (**g**) stimulation in dTRPA1 expressing cells supplemented with solvent (control), 100 μM
908 16-AG, or 18-AG. Each point represents a biological replicate. The number of replicates (n) is
909 shown in the panels. Data are presented as mean ± SEM. *$p < 0.05$; Dunnett test (vs. control).
910 Source data are provided as a Source Data file.

911

912 **Fig. 5 AGPS modulates mechanosensory behaviors.**

913 **a** Distribution of scored responses to gentle touch with a nickel–titanium filament in $w^{1118}$ (control)
914 and $AGPS^{KO}$ late third instar larvae (n = 4). 0: no response, 1: hesitation, 2: turn or withdrawal of
915 the anterior segments, 3: single reverse contractile, or 4: multiple reverse contraction. **b** Responses
916 to different forces applied with von Frey filaments (20.1, 47.0, and 70.0 mN) in $w^{1118}$ (control, n =
917 4 or 5) and $AGPS^{KO}$ late third instar larvae (n = 4 or 5). **c** Responses to a von Frey filament (20.1
918 mN) in control (*UAS-AGPS RNAi*/+, n = 5) and *AGPS* knockdown using *PIEZO-GAL4* (n = 5),
919 *TRPA1-CD*$^{GAL4}$ (n = 5), *ppk-GAL4* (n = 5), and *pain-GAL4* (n = 6). Data are presented as mean ±
920 SEM. *p < 0.05, **p < 0.01; student's t-test (**b**) or Dunnett test (vs. control) (**c**). Source data are
921 provided as a Source Data file.
922
923 **Fig. 6 ePLs modify dPIEZO activity in *Drosophila* cells.**
924 **a–c** Representative Fura-2 imaging data for PIEZO in control S2R+ cells and cells supplemented
925 with 100 μM 18-AG. **a** Typical ratiometric images before (Basal, at 60 s) and after 10 μM Yoda1
926 application (Yoda1, at 360 s), and after 5 μM ionomycin application (Ionomycin, at 540 s) in
927 dPIEZO expressing cells (upper) and dPIEZO expressing cells supplemented with 100 μM 18-AG
928 (lower). **B, c** Representative calcium level traces in dPIEZO expressing cells (**b**) and 18-AG
929 supplemented dPIEZO expressing cells (**c**). **d, e** Proportion of cells responding to Yoda1 (Δratio >
930 2) (**d**) and maximum Δratio response to Yoda1 normalized by the ionomycin response (**e**) in
931 dPIEZO expressing cells (control, n = 10) and 18-AG supplemented dPIEZO expressing cells (18-
932 AG, n = 10). Each point represents a biological replicate; 25—40 cells were analyzed in each assay.
933 Data are presented as mean ± SEM. *p < 0.05, **p < 0.01; Student's t-test. Source data are
934 provided as a Source Data file.
935
936 **Fig. 7 ePLs alters membrane properties of *Drosophila* cells.**
937 **a** Measurement of membrane tension by AFM in S2R+ cells (control) and cells supplemented with
938 100 μM 18-AG. Data were acquired from 242 different regions of 24 control cells and 213 different
939 regions of 27 cells supplemented with 18-AG. The red horizontal lines represent the median and
940 each point the averaged Young's modulus (Pa) of each region. **b** Measurement of membrane
941 tension by FLIM imaging using Flipper-TR in control (n = 45) and 100 μM 18-AG supplemented
942 S2R+ cells (n = 40). The average fluorescent lifetime of each cell is shown as well. Red horizontal
943 lines represent the median and each point a biological replicate. **c** Representative pseudo color

944 images of LipiORDER loaded control (upper) and 100 μM 18-AG supplemented S2R+ cells
945 (lower). Green fluorescence intensity (left, 450—550 nm), red fluorescence intensity (middle,
946 550—650 nm), and radiometric images of red to green fluorescence intensity (right, R/G ratio). **d**
947 Fluorescence emission spectrum from 450 nm to 650 nm with a 25-nm interval in control (black,
948 n = 46) and 100 μM 18-AG supplemented S2R+ cells (red, n = 45). Data are presented as mean ±
949 SEM. **e** Quantification of red/green fluorescence ratio (R/G ratio). Each value indicates the average
950 R/G ratio of a single cell. Red horizontal lines represent the median and each point a biological
951 replicate. *$p < 0.05$, ***$p < 0.001$; Mann–Whitney U-test. Source data are provided as a Source
952 Data file.

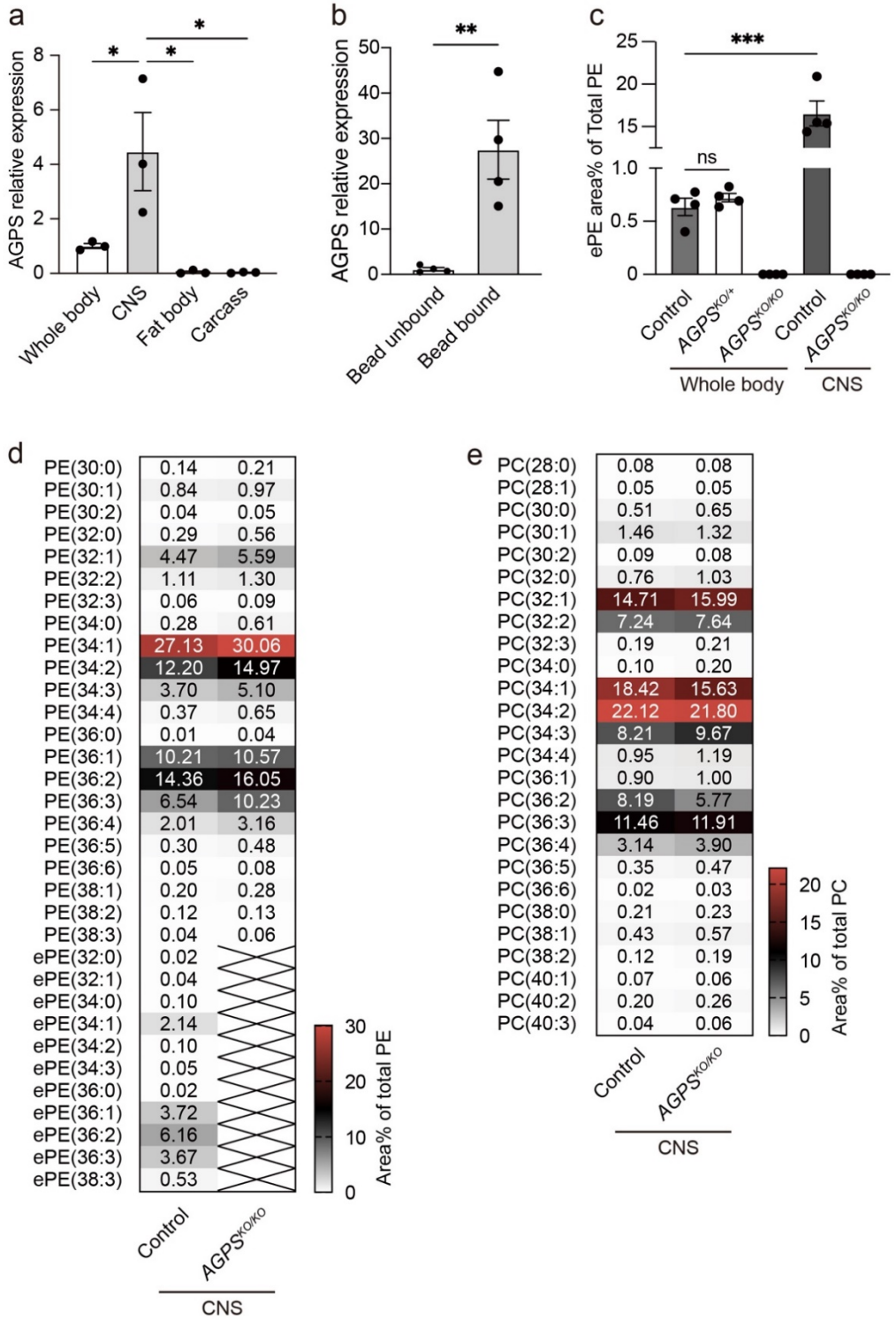


Fig1 Suito et al. 2023

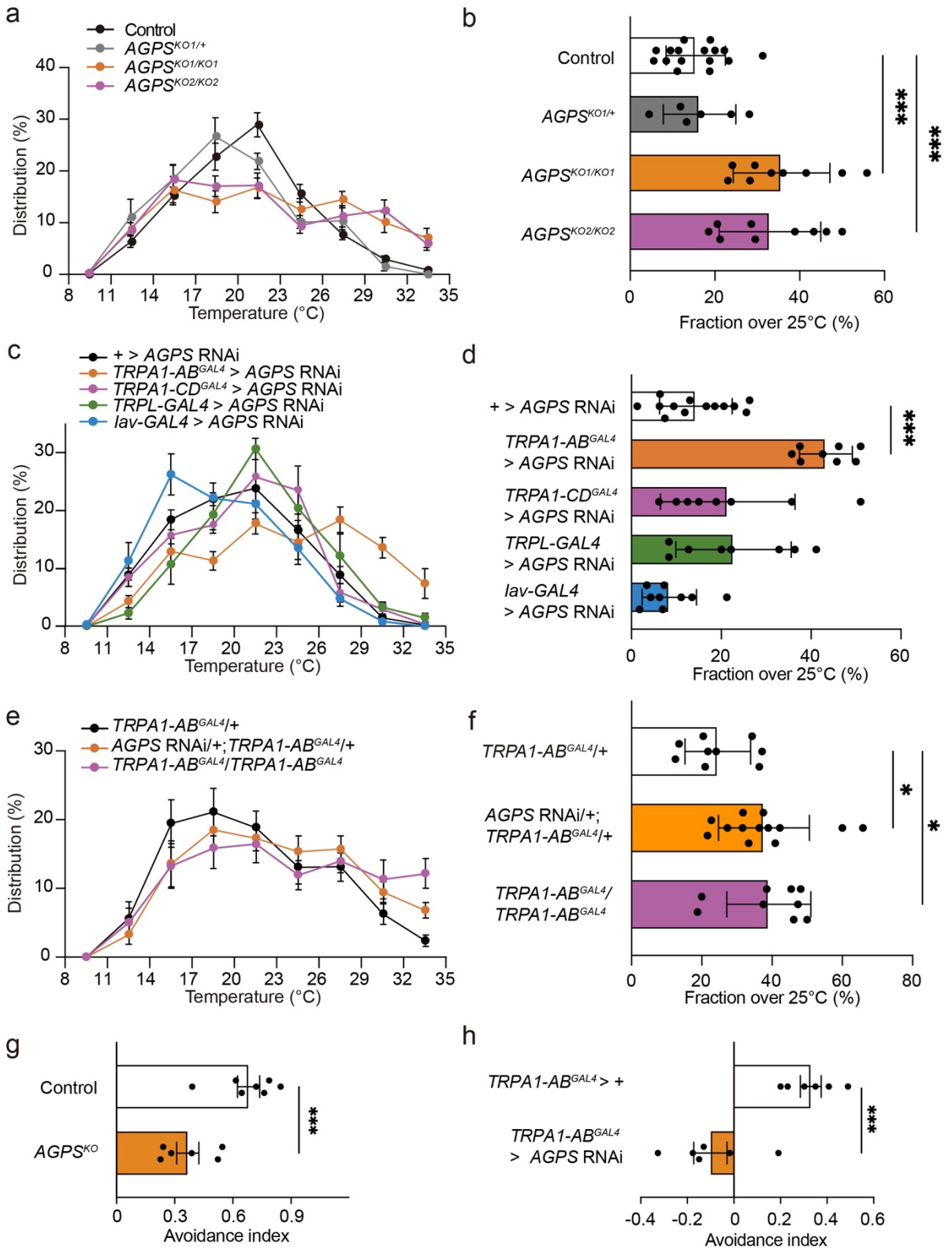


Fig2

Suito et al. 2023

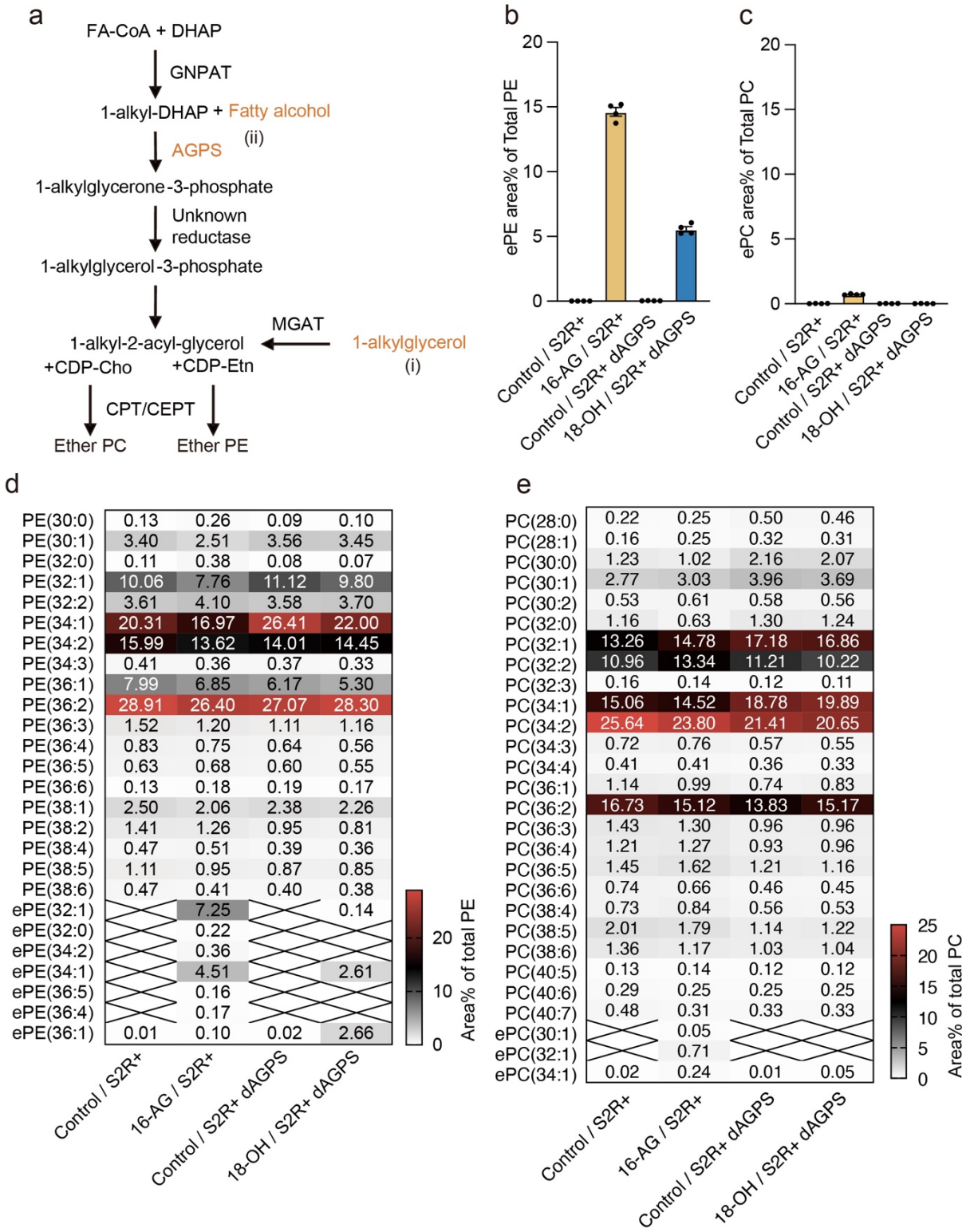


Fig3

Suito et al. 2023

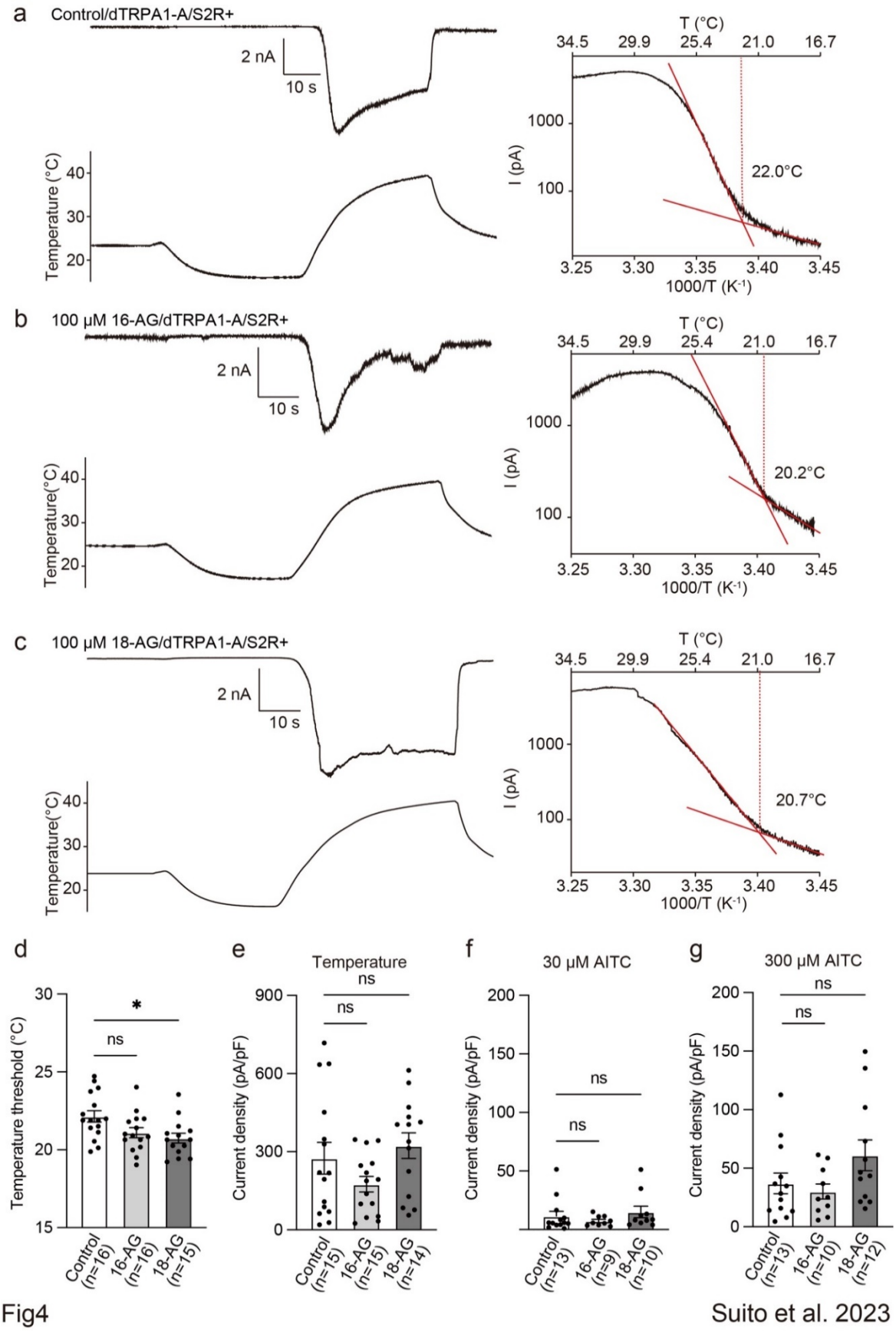


Fig4

Suito et al. 2023

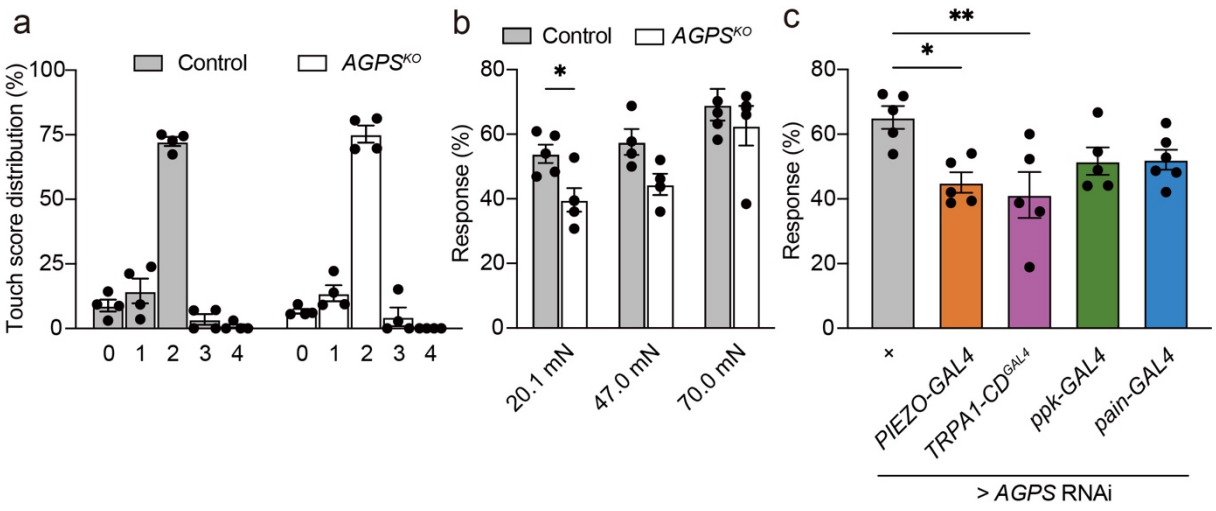


Fig5 Suito et al. 2023

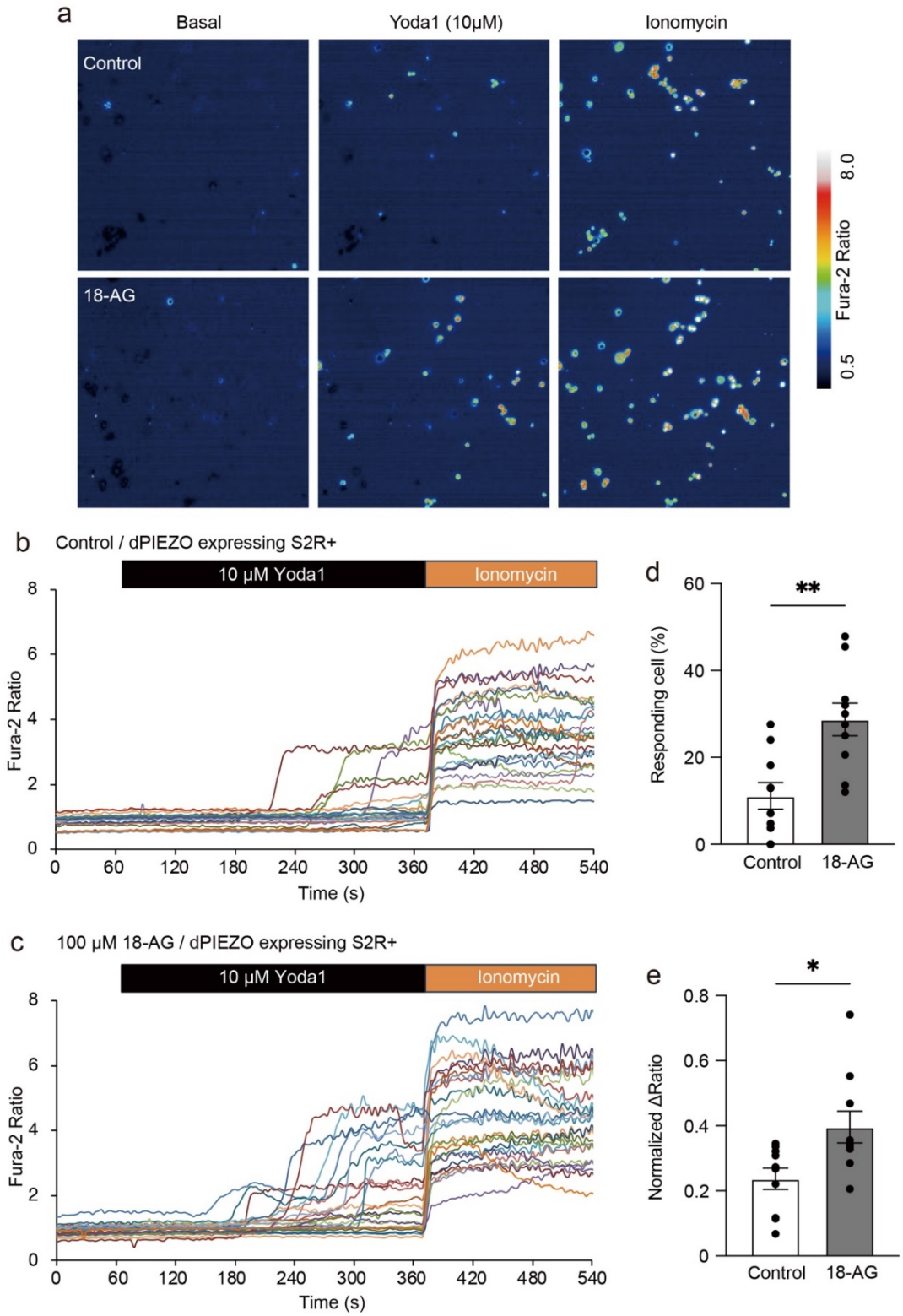


Fig6

Suito et al. 2023

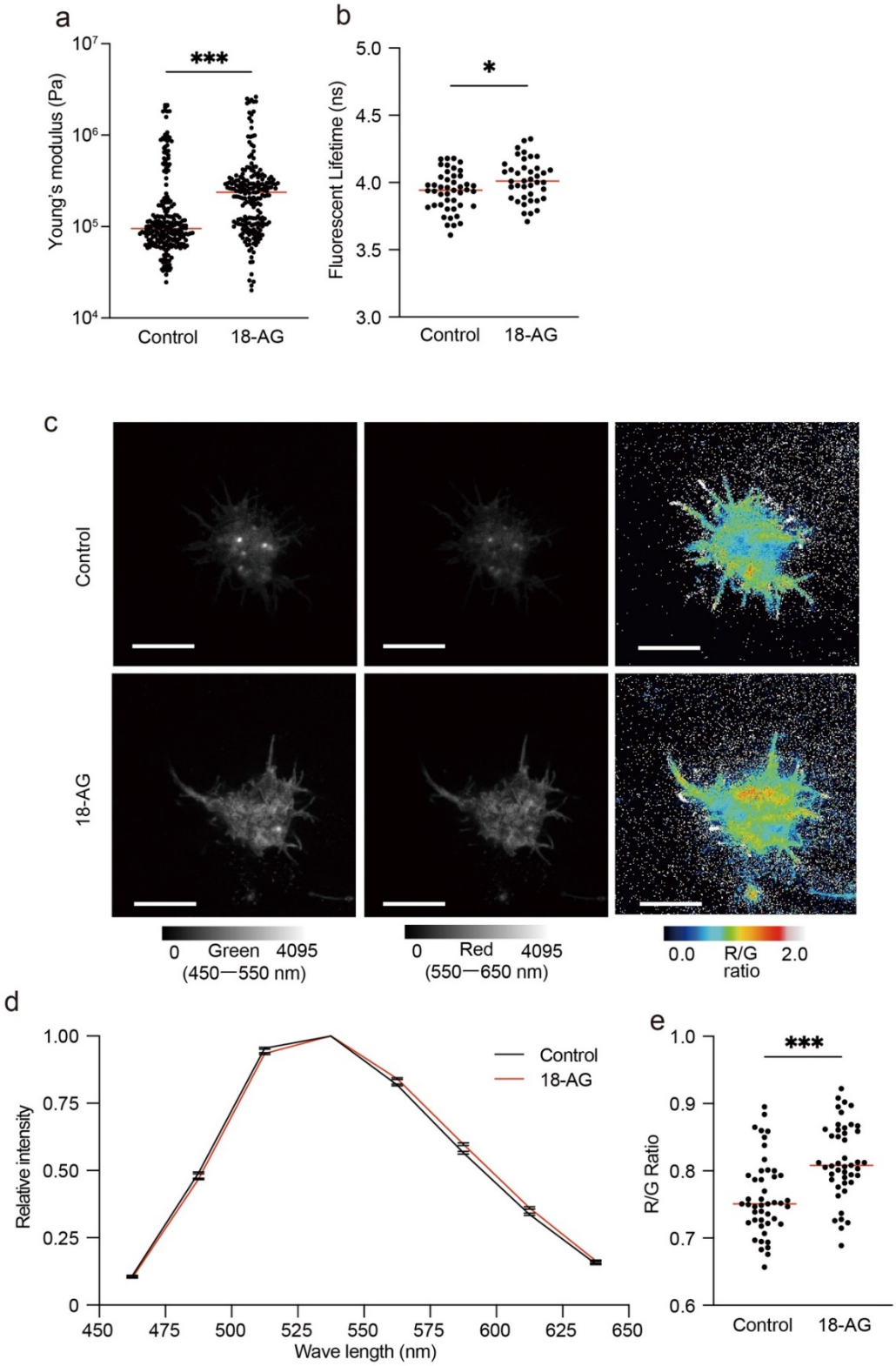


Fig7

Suito et al. 2023